Supplementary information

Triple-element compound-specific stable isotope analysis (3D-CSIA): added value of Cl isotope ratios to assess herbicide degradation

Clara Torrentó[1†*], Violaine Ponsin[1‡], Christina Lihl[2], Thomas B. Hofstetter[3], Nicole Baran[4], Martin Elsner[2,5], Daniel Hunkeler[1]

[1]Centre of Hydrogeology and Geothermics (CHYN), University of Neuchâtel, 2000 Neuchâtel, Switzerland

[2]Helmholtz Zentrum München, Institute of Groundwater Ecology, 85764 Neuherberg, Germany

[3]Eawag, Swiss Federal Institute of Aquatic Science and Technology, 8600 Dübendorf, Switzerland

[4]BRGM, Bureau de Recherches Géologiques et Minières, 45060, Orléans CEDEX 02, France

[5]Technical University of Munich, Chair of Analytical Chemistry and Water Chemistry, 81377 Munich, Germany

[*]Corresponding author: Clara Torrentó, Phone: +34 93 403 37 73, e-mail: clara.torrento@gmail.com

[†]Present Address: Grup MAiMA, Departament Mineralogia, Petrologia i Geologia Aplicada, Facultat de Ciències de la Terra, Universitat de Barcelona (UB), C/ Martí i Franquès s/n, 08028, Barcelona, Spain.

[‡]Present address: Département des sciences de la Terre et de l'atmosphère, Université du Québec à Montréal, 201 avenue du Président Kennedy, Montréal, QC, Canada.

Content (36 pages):

Content of Figures

Content of Tables

1. Chemicals and additional details for the experiments

ACETO (CAS no 34256-82-1), METO (CAS no 51218-45-2) and ATR (CAS no 1912-24-9) Pestanal-quality standards and the internal standard terbuthylazine (CAS no 5915-41-3) were purchased from Sigma-Aldrich. 2-hydroxy-acetochlor (HACETO, CAS no 60090-47-3) and 2-hydroxy-metolachlor (HMETO, CAS no 131068-72-9) 100 µg/mL Pestanal-quality solutions in acetonitrile and 2-hydroxy-atrazine (HATR, CAS no 2163-68-0) Pestanal-quality standard were purchased from LGC Standards GmbH. The in-house isotope standards used for spiking the hydrolysis experiments and for isotope measurements are detailed in **Table S1**. Carbon and nitrogen isotope ratios of the in-house standards were determined by Elemental Analyzer (EA)-IRMS based on two-point normalization using international reference materials (Torrentó et al., 2019), whereas chlorine isotope ratios were determined by GC interfaced with multiple-collector inductively coupled plasma MS (GC-MC-ICPMS) (Lihl et al., 2019). The METO standard used for spiking the soil degradation experiments was purchased from Dr. Erhenstorfer.

Table S1. Isotope ratios of ACETO, METO and ATR in-house isotope standards. SMOC $\delta^{37}Cl$ values were determined by GC-MC-ICPMS (Lihl et al., 2019). $\delta^{15}N$ values were determined through injection in an EA-IRMS as described by Torrentó et al. (2019). $\delta^{13}C$ values were determined either through injection in an EA-IRMS[a] or through injection in a GC-IRMS[b] as explained elsewhere (Ponsin et al., 2019).

Compound	Standard	$\delta^{37}Cl \pm SD$ [‰]	$\delta^{13}C \pm SD$ [‰]	$\delta^{15}N \pm SD$ [‰]	Purpose
Acetochlor	ACETO-I	0.3 ± 0.3	-27.8 ± 0.2[b]	n.d.	Cl isotope measurement
	ACETO-F	18.5 ± 0.2	-16.4 ± 0.2[b]	n.d.	Cl isotope measurement
	ACETO_A	-0.1 ± 0.2	-25.0 ± 0.1[a]	0.5 ± 0.1	C and N isotopes measurement
Metolachlor	METO-I	-4.3 ± 0.2	-28.6 ± 0.1[b]	n.d.	Cl isotope measurement
	METO-F	5.1 ± 0.3	-22.5 ± 0.1[b]	n.d.	Cl isotope measurement
	METO_A	0.0 ± 0.1	-30.4 ± 0.1[a]	0.3 ± 0.1	C and N isotopes measurement
Atrazine	ATR #4	-0.9 ± 0.2	-26.4 ± 0.1[a]	n.d.	Cl isotope measurement
	ATR #11	3.6 ± 0.4	-28.2 ± 0.1	-0.59 ± 0.1	Cl isotope measurement
	ATR_A	-0.9 ± 0.2	-28.4 ± 0.2[a]	-1.45 ± 0.1	C and N isotopes measurement

n.d. not determined

1 mg/mL standard stock solutions were prepared in ethyl acetate (EtAc) and stored in the dark at -18°C. For concentration analyses, working solutions were prepared by dilution of the stock solution in ethanol (EtOH). Calibration solutions were prepared in methanol (MeOH):ultrapure water (70:30 v/v) mixture with concentrations ranging from 10 to 1000 µg/L. Standards used for chlorine isotope analyses were prepared from 100-250 mg/L working solutions diluted in EtAc to a final concentration comprised between 2 and 40 mg/L. For carbon and nitrogen isotope analyses, 10 to 14 g/L solutions of the in-house standards were diluted in EtAc to final concentrations ranging between 30 and 800 mg/L. All solutions were renewed every 6 months. MeOH, EtAc and EtOH of analytical grade were used. Ultrapure water was prepared by ultrafiltration with a Millipore DirectQ apparatus (Millipore, Bedford, MA, USA).

Buffer solutions for the hydrolysis experiments were prepared at pH 3 (0.2 M Na_2HPO_4 with 0.1 M citric acid), pH 7 (0.05 M Na_2HPO_4) and pH 12 (0.05 M Na_2HPO_4 with 0.1 M NaOH). Aliquots from the experiments were extracted by SPE as explained elsewhere (Ponsin et al., 2019) using 6-mL SPE cartridges filled with 0.2 g of the sorbent Sepra ZT. Empty polyethylene 6-mL Grace Pure™ cartridges and matching polyethylene frits (20-µm pore size) were obtained from Grace (Loreken, Belgium). The styrene-divinylbenzene sorbent Sepra ZT (760-820 m^2/g surface area) and a 12-positions SPE vacuum manifold station were purchased from Phenomenex (Torrace, CA, USA).

Soil samples from the soil degradation experiments were collected in the Ariège alluvial plain (South West of France). Soil M, from the municipality of Montaut, corresponds to a silty soil (to silty-sandy-clay) developed on the alluvium of the Ariège central low terrace. Soil V, from the municipality of Pamiers, is a not very evolved soil consisting on clayey-silty sands that developed on the alluvium of the Ariège low plain. Selected physico-chemical properties of the two soils are shown in **Table S2**. The two soils were cultivated with wheat in the year of sampling. Both soils were sampled from 0 to 25 cm depth.

Table S2. Selected characteristics of the two soils used in the soil degradation experiments.

	Soil M	**Soil V**
Origin	Montaut	Pamiers
	43° 11' 23.496''N;	43° 8' 42.248''N;
	1° 39' 59.918''E	1° 38' 5.967''E"
Clay (g/kg soil)	117	157
Fine silt (g/kg soil)	221	163
Coarse silt (g/kg soil)	224	167
Fine sand (g/kg soil)	253	157
Coarse sand (g/kg soil)	172	339
Clay (< 2 µm) (%)	11,9	16.0
Silt (2 - 50 µm) (%)	45.1	33.6
Sand (50 - 2000 µm) (%)	43.1	50.5
Soil texture	Sandy clay loam	Clayey-silty sand
Organic matter (g/kg soil)	12.8	17.2
Cation exchange capacity (CEC) (meq/100 g)	74	74
pH (water)	6.9	5.9
pH (KCl)	5.9	4.4

Soil samples from the soil degradation experiments were extracted using a QuEChERS® extraction kit (EN 15662 buffered method, Agilent). Briefly, 5 g of soil were place in a 50 mL tube and 80 µL of a surrogate (5 mg/L metolachlor-d6 in acetonitrile, an amount 20-70 times smaller than the non-labelled compound), 8 mL of 30 mM KH_2PO_4 and 10 mL of 5% HCOOH acetonitrile were added. The tube was shaken manually during 30 seconds and the extraction salts (4 g $MgSO_4$, 1 g NaCl, 1 g sodium citrate, 0.5 g disodium citrate sesquihydrate) were added. The mixture was agitated during 1 min and centrifuged (4000 rpm) during 5 minutes. The supernatant was transferred to another tube and the extract volume was adjusted to 2 mL with acetonitrile. Extractions were performed in triplicate and the three resulting extracts were combined in one.

Considering a pseudo-first order reaction, rate constants (k') were calculated through regression of the natural logarithm of the fraction of the parent compound against time following **Eq. (S1)**. Uncertainty was obtained from 95% confidence intervals (95% CI).

$$ln\left(\frac{C_t}{C_0}\right) = k' \times \mathrm{t} \qquad \textbf{Eq (S1)}$$

The half-life ($t_{1/2}$) was calculated as follows:

$$t_{1/2} = \frac{\ln(2)}{k'} \qquad \textbf{Eq (S2)}$$

The uncertainty of half-life values was estimated by error propagation.

2. Analytical methods

Concentration analyses

For the hydrolysis experiments, concentrations of parent compounds (ACETO, METO, ATR) and hydroxylated degradation products (HACETO, HMETO, HATR) were determined by ultra-high-pressure liquid chromatography quadrupole time of flight mass spectrometry (UHPLC-QTOF-MS) following a method described elsewhere (Torrentó et al., 2019). Briefly, a Synapt G2 Q-TOF MS (Waters) was operated in positive ionization mode using the MS full scan mode over a mass range of 50-600 Da with a scan time of 0.4 sec. The Q-TOF was coupled to an Acquity UPLC™ system (Waters) and an Acquity UPLC BEH C18 column (50 mm × 2.1 mm × 1.7 µm, Waters) was used at a flow rate of 0.4 mL/min in gradient mode. A guard column (5 mm × 2.1 mm × 1.7 µm) of identical phase chemistry was placed before the column. The mobile phase consisted of two solvents: solvent A (water and formic acid 0.05%) and solvent B (acetonitrile and formic acid 0.05%). The following gradient was used: 2-65% B in 4.5 min, 65-100% B in 1 min, holding at 100% B for 1.5 min and re-equilibration at 2% B for 1.5 min. Quantification was performed by the internal standard method, based on peak areas, using terbuthylazine as internal standard. For quantification, extracted ion chromatograms were generated using mass windows of 0.02 Da around the mass-to-charge ratios (m/z) of the analytes. Note that under alkaline hydrolysis, the equilibrium of the two tautomers of HATR (Lerch and Donald, 1994) resulted in a double peak for this compound. Peak 1 was used for quantification. More details are shown in **Table S3**. The limits of quantification were 14 µg/L for ACETO, 4.4 µg/L for METO, 3 µg/L for ATR, 16 µg/L for HACETO, 2.5 µg/L for HMETO and 3 µg/L for HATR.

Table S3 also shows tentatively identified non-hydroxylated degradation products. Formal identification and quantification of these products was not possible in the absence of available standards at the laboratory at the time analyses were made. Tentative identification occurred when an expected ion was identified with mass error below 5 ppm, together with its characteristic isotopic pattern (if present), and one or more fragment ions were in agreement with data reported and compatible with the chemical structure of the candidate.

Table S3. Parameters for UHPLC-QTOF-MS analysis: quantifier and qualifier ions, retention time and the instrument method detection (LOD) and quantification (LOQ) limits. *denotes a putative structure.

Compound	quantifier ion (m/z)	qualifier ion (m/z)	retention time	LOD (µg L^{-1})	LOQ (µg L^{-1})
Acetochlor (ACETO)	224.080	284	4.63	4.8	14.0
Metolachlor (METO)	284.141	306	4.57	1.5	4.4
Atrazine (ATR)	216.103	218	3.33	1.0	3.0
2-hydroxy-acetochlor (HACETO)	252.159	174	3.60	5.3	16.0
2-hydroxy-metolachlor (HMETO)	266.175	266	3.66	0.9	2.5
2-hydroxy-atrazine (HATR) – peak 1	198.136	156	1.66	1.0	3.0
2-hydroxy-atrazine (HATR) – peak 2	198.136	156	1.87	-	-
2-chloro-N-(2-ethyl-6-methylphenyl)acetamide (CMEPA) (**I**)*	212.084	214	3.34	-	-
N-(2-ethyl-6-methylphenyl)-2-hydroxyacetamide (**II**)*	194.119	216	2.30	-	-
N-(ethoxymethyl)-N-(2-ethyl-6-methylphenyl)-2-methoxyacetamide (**III**)*	192.141	266	3.94	-	-

4-(2-Ethyl-6-methylphenyl)-5-methyl-3-morpholinone (Metolachlor-morpholinone) (**IV**)*	234.149	256	3.35	-	-
N-(2-ethyl-6-methylphenyl)-2-methoxy-N-(1-methoxypropan-2-yl)acetamide (**V**)*	280.192	302	3.96	-	-
2-Methoxy-4-isopropylamino-6-ethylamino-S-triazine (atraton) (**VI**)*	212.152	213	2.22	-	-

For the soil degradation experiments, METO and metabolites concentrations were determined by UPLC-triple quadrupole mass spectrometer (UPLC-QqQ-MS Quattro TQD, Waters). Simazine-d10 was used as internal standard. Chromatographic separation was done with a Waters Acquity UPLC BEH C18 column (2.1 mm x 150 mm x 1.7µm) maintained at 60 °C. The mobile phase was a gradient of water/0.007% formic acid (eluent A) and methanol/0.007% formic acid (eluent B) with a flow rate of 0.3 mL/min. The elution gradient started with 90% eluent A, maintaining isocratic conditions for 1 minute. Then eluent B increased to 100% in 8 minutes and was maintained for 2 minutes. Finally, initial conditions were reached again in 0.50 minutes with a re-equilibrium time of 2 minutes to restore the column. The injection volume was 2 µL. The ion source parameters are set to: desolvation temperature 650 °C, desolvation gas flow 800 L/h, cone gas 50 L/h, and source temperature 150 °C. Other mass spectrometry parameters are reported in **Table S4**. The limit of quantification was 20 µg/L for METO.

Table S4. Mass spectrometric parameters for UPLC-QqQ-MS analysis for electrospray ionization in positive and negative mode (ESI+/ ESI-).

Ionization mode	molecule	Cone voltage (V)	Transition 1	Collision energy (eV) 1	Transition 2	Collision energy (eV) 2
ESI +	Simazine-d10 (IS)	35	212> 105	25	212> 137	20
	Metolachlor (METO)	25	284> 176	25	284> 252	15
	Metolachlor-d6 (SURR)	25	290> 182	25	290> 258	13
ESI -	Metolachlor OXA	20	278> 174	20	278> 206	11
	Metolachlor ESA	40	328> 80	33	328> 121	25

Chlorine isotope analysis

Chlorine isotope ratios were measured following Ponsin et al. (2019), using the two-point calibration approach and applying corrections to take into account fragments with two ^{13}C atoms. Briefly, chlorine isotope ratios were determined using an Agilent 7890 A GC coupled to an Agilent 5975 qMS. 1 µL of sample was injected splitless in a split/splitless injector maintained at 250°C. A DB-17ms column (30 m x 0.25 mm x 0.25 µm, Agilent) operated in constant flow mode (1.2 mL/min of helium) was used for separation. The oven program was 60°C (1 min), 30°C/min to 190°C (3 min), 3°C/min to 210°C (3 min). The interface was maintained at 280°C, the ion source at 230°C and the quadrupole at 150°C. Selected-ion monitoring measurements were performed, and the following ions were monitored: m/z 223 and 225 (ACETO), m/z 238 and 240 (METO) and m/z 200 and 202 (ATR). A dwell time of 30 ms was applied. Ten injections of each sample were performed and two external working standards, also injected ten times each, were interspersed along the sequence to correct for potential drift. Concentrations of external standards were adjusted to those of the samples with a 20% tolerance.

Carbon and nitrogen isotope analysis

Carbon and nitrogen isotope ratios in the extracts from the hydrolysis experiments were measured by GC-IRMS, as explained elsewhere (Torrentó et al., 2019), with a TRACE GC Ultra coupled to a Delta V Plus IRMS via a GC Combustion III interface (all from Thermo Fisher Scientific). Briefly, a self-made Ni/Ni/Pt reactor was operated at 1180°C and reoxidized for 20 min with a continuous O_2 stream after every measurement. For N isotope analysis, a standard reduction reactor (Thermo) was also used at 650°C and liquid N_2 was used for cryogenic trapping of CO_2. 1 µL for C and 5 µL for N were injected in a split/splitless injector operated for 1 min in splitless and then in split mode with a split flow of 50 mL/min at a temperature of 230°C. A Rxi-5ms column (60 m x 0.32 mm x 1 µm, Restek) operated at constant pressure (200 kPa helium) was used for separation. The oven temperature program was 50°C/min from 80 to 230°C, 2°C/min to 270°C (10 min) and 20°C/min to 280°C (10 min). In-house standards were interspersed in each sample sequence to ensure the stability of the measurements during the course of sample analyses. Samples and standards were diluted to a similar concentration and measured in triplicate.

Carbon isotope ratios in the soil extracts were measured by GC-IRMS with a Trace GC Ultra coupled to a Delta Plus XP IRMS via a GC Combustion III interface (Thermo Finnigan). A NiO/CuO/Pt reactor was operated at 940°C. 1 µL was injected in a split/splitless injector operated for 1 min in splitless and then in split mode at a temperature of 250°C. A DB-17ms column (60 m x 0.32 mm x 1 µm, Agilent) operated in constant pressure mode was used for separation. The oven program was 80°C (1 min), 50°C/min to 230°C (0 min), 2°C/min to 270°C (10 min). In-house standards were interspersed in each sample sequence to ensure the stability of the measurements during the course of sample analyses. Samples and standards were diluted to a similar concentration and measured in quadruplicate.

3. Determination of AKIEs

AKIE values were calculated following **Eq. (3)** of the main text, where n is the number of atoms of the considered element, x is the number of these atoms located at the reactive site/s, z is the number of atoms located at the reactive site/s and being in intramolecular competition. The values for n, x, and z (**Table S5**) were chosen depending on the considered reaction mechanism.

Table S5. Parameters used for AKIEs calculation. na= not analyzed.

Compounds	Degradation	Chlorine			Carbon			Nitrogen		
		n	x	z	n	x	z	n	x	Z
Acetochlor	Acidic hydrolysis	1	1	1	14	1	1	1	1	1
	Alkaline hydrolysis	1	1	1	14	1	1	1	1	1
Metolachlor	Acidic hydrolysis	1	1	1	15	1	1	1	1	1
	Alkaline hydrolysis	1	1	1	15	1	1	1	1	1
	Soil degradation	1	1	1	15	1	1	na	na	na
Atrazine	Acidic hydrolysis	1	1	1	8	1	1	5	3	3
	Alkaline hydrolysis	1	1	1	8	1	1	5	5	1

Acetochlor and metolachlor hydrolysis

For both acidic, alkaline and neutral hydrolysis (nucleophilic substitution at the C-Cl bond position as the main degradation mechanism), primary normal isotope effect is expected for carbon and chlorine. As there is only one C-Cl bond, x = z = 1 was used for both $AKIE_C$ and $AKIE_{Cl}$ determination. If there is any isotope fractionation in nitrogen, it is expected to be secondary and, since there is only one N atom, x = z = 1 was used for $AKIE_N$ determination.

Metolachlor degradation in soil

Thiolytic S_N2 type nucleophilic substitution at the C-Cl bond position is considered. As there is only one C-Cl bond, x = z = 1 was used for both $AKIE_C$ and $AKIE_{Cl}$ determination. Therefore, primary normal isotope effect is expected for carbon and chlorine.

Atrazine hydrolysis

For acidic hydrolysis, protonation of a N atom of the heterocyclic ring followed by nucleophilic substitution of the chlorine atom by a hydroxyl group via a S_NAr addition-elimination pathway is considered (Meyer et al., 2009). Therefore, primary inverse isotope effect is expected for nitrogen, whereas primary normal isotope effect is expected for carbon and chlorine. As the three N atoms of the heterocyclic ring are equivalent and compete for protonation, x = z = 3 was used for $AKIE_N$ determination. As there is only one C-Cl bond, x = z = 1 was used for both $AKIE_C$ and $AKIE_{Cl}$ determination.

For alkaline hydrolysis, a direct substitution of the chlorine atom is proposed. Therefore, a primary normal isotope effect for carbon and chlorine and a secondary normal isotope effect for nitrogen is expected. As there is only one C-Cl bond, x = z = 1 was used for both $AKIE_C$ and $AKIE_{Cl}$ determination. It was assumed that all the nitrogen atoms are embedded in the aromatic π-system that is disturbed by reaction at the C-Cl position and thus all the nitrogen atoms may contribute simultaneously with a secondary isotope effect to observable fractionation (Meyer et al., 2009). Therefore, x = n = 5 and z = 1 was used for the determination of an average $AKIE_N$ value.

4. Spiked tests for soils experiments

Two different tests were performed for assessing carbon and chlorine isotope fractionation during soil extraction and concentration: "spiked soils", in which the two soils were spiked with METO and extracted immediately (for assessing the potential isotope fractionation associated with the whole procedure), and "spiked extracts", in which extracts from the two soils were spiked with METO (for assessing the potential isotope fractionation associated with the evaporation and reconstitution of the extracts, the effect of soil matrices and the effect of METO mass).

For spiked soils, each soil (50 g) was spiked with METO to a final concentration of approximately 2.5 µg/g. These tests were performed in duplicate. Three aliquots of 15 g soil were extracted using the procedures described in the main text. The three extracts were combined in one (6 mL acetonitrile-water), which was then dried over N_2 flow to dryness and reconstituted in an appropriate volume of ethyl acetate (200-300 µL) for injection into the GC-IRMS and the GC-qMS. Final recoveries ranged between 40 and 90% (**Table S6**).

For spiked extracts, aliquots of 15 g of the two soils were extracted using the procedures described in the main text. 4 mL-aliquots of the acetonitrile-water extracts were then spiked at two different concentration levels (4000 and 8000 µg/L METO, which should correspond to 16 or 32 µg, respectively). The extracts were then dried over N_2 flow to dryness and reconstituted in an appropriate volume of ethyl acetate (200-300 µL) for injection into the GC-IRMS and the GC-qMS. Final recoveries were > 80% (**Table S6**).

Table S6. Recovery and carbon ($\Delta\delta^{13}C$) and chlorine ($\Delta\delta^{37}Cl$) isotopic shifts associated with extraction for "spiked soils" and "spiked extracts" tests. $\Delta\delta^{13}C$ and $\Delta\delta^{37}Cl$ values were determined as the difference between the measured $\delta^{13}C$ and $\delta^{37}Cl$-METO value in the extract and the mean $\delta^{13}C$ and $\delta^{37}Cl$ values of the spiked METO standard obtained by replicate injections in the GC-IRMS and the GC-qMS, respectively. The error given for $\Delta\delta^{13}C$ and $\Delta\delta^{37}Cl$ was calculated by error propagation.

	Spiked mass (µg/50 µg soil)	**Exact mass in the extract (µg)**	**Recovery (%)**	**$\Delta\delta^{37}Cl$ (‰)**	**$\Delta\delta^{13}C$ (‰)**
Spiked soil, soil M	134	40	39	3.3±0.3	-0.5±0.4
	140	42	57	3.4±0.3	-0.8±0.1
Spiked soil, soil V	141	42	59	2.5±0.3	-1.1±1.1
	126	38	88	3.6±0.3	-1.2±0.5
Spiked extracts, soil M	*8000 µg/L*	36	114	0.7±0.2	2.2±0.7
	4000 µg/L	17	105	2.5±0.2	2.2±0.8
Spiked extracts, soil V	*8000 µg/L*	26	80	1.3±0.2	3.1±0.6
	4000 µg/L	21	132	1.9±0.2	1.8±0.1

The whole procedure ("spiked soils") produced a systematic isotope fractionation ($\Delta\delta^{37}Cl$= between +2.5 and +3.5‰) for Cl isotopes, which is the same for the two soils (**Figure S1**). The evaporation + reconstitution steps ("spiked extracts") were responsible of a Cl isotope shift between +0.7 and +2.5‰.

The effect of the whole extraction procedure on METO-$\delta^{13}C$ values was insignificant ($\Delta\delta^{13}C$ <1‰, within error, **Figure S1**), while the evaporation + reconstitution steps seemed to introduce a systematic shift around +2‰. This difference in behavior between the two spiked tests may be attributable to the fact that METO used for the spiked soils was dissolved in a mixture of water and acetonitrile while METO in the spiked extracts was dissolved in methanol. Because no tests were done on METO masses < 17 µg, samples with METO masses below this value were not considered for isotope analyses.

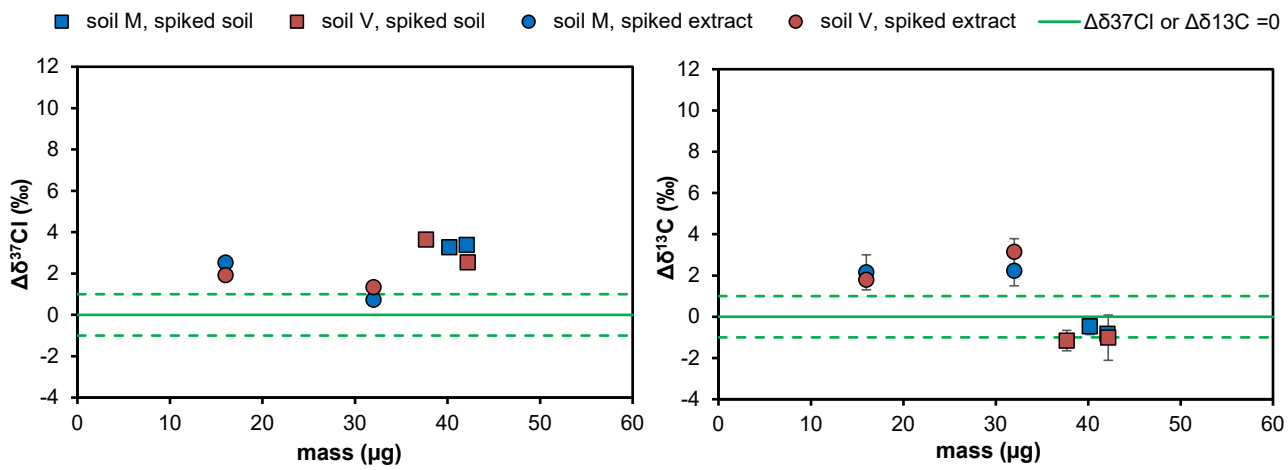

Figure S1. Deviation of Cl ($\Delta\delta^{37}Cl$) and C ($\Delta\delta^{13}C$) isotope signature for "spiked soils" and "spiked extracts" tests in both soils. Green lines correspond to the measured Cl and C isotope ratios for standards used to spike the soils and the extracts. The dashed green lines shown the uncertainty of ±1‰. Error bars display the uncertainty calculated by error propagation.

5. Estimation of the influence of deuterated metolachlor on the measured carbon isotope signature

For the soil degradation experiments and the spiked soil tests, where METO-d6 was added as a surrogate prior to the extraction, the carbon isotope signature of METO-d6 could potentially affect the measurement of δ^{13}C-METO by GC-IRMS. It should be noted that this effect is not expected for δ^{37}Cl determinations, since they are based on GC-qMS analysis of selected ions.

A simple sensitivity assessment was performed to evaluate the potential effect of the carbon isotope signature of the deuterated metolachlor on δ^{13}C of the remaining METO mass during its biodegradation in soil. For that purpose, a ε_C of -2‰ was considered, based on the previously reported range for METO degradation in soils (from -1.4 to -1.8‰, Alvarez-Zaldívar et al., 2018; Meite, 2018). A linear isotope mixing model for two members was used (**Eq. S3**), where δ_{tot} is the carbon isotope signature that would be measured by GC-IRMS (*i.e.*, isotope signature of the mixture), δ_{d6} and δ_{meto} are the carbon isotope signature of the deuterated compound and the metolachlor, respectively, and X_{d6} and X_{meto} are their fractional contribution to the mixture of the deuterated surrogate and the metolachlor, respectively (*i.e.*, $X_{d6} + X_{meto} = 1$). For a conservative estimation, we assumed a difference between the carbon isotope signature of the spiked METO and the METO-d6 used as a surrogate of ±10‰. Doses of 3.3 µg/g soil for the spiked METO and 0.08 µg/g soil for the surrogate were considered, which for extractions of 15 g soil correspond to 50 µg METO and 1.2 µg METO-d6.

$$\delta_{tot} = \delta_{d6} X_{d6} + \delta_{meto} X_{meto} \qquad \textbf{Eq (S3)}$$

The theoretical trends for the δ^{13}C of the residual fraction of METO during its biodegradation in soil and for the estimated δ_{tot} are shown in **Figure S2.** The deviation between δ_{meto} and δ_{total} is within measurement uncertainty (±0.5‰), except when the fraction of METO-d6 is higher than 5%, which in this case corresponds to a METO residual fraction lower than 0.4. The criteria of <5% of METO-d6 was thus followed for selecting samples from the soil experiments for carbon isotope analysis.

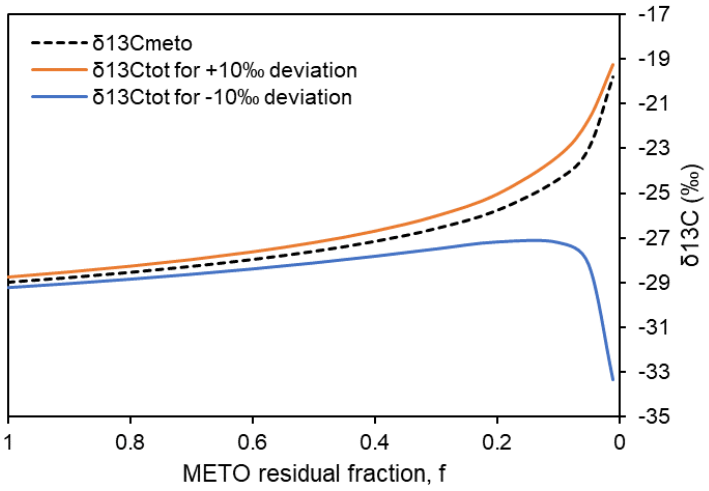

Figure S2. Theoretical trends of δ^{13}C-METO variation during its degradation in soil following the Rayleigh model and using a ε_C of -2‰ (dashed line) and for expected δ^{13}C that would be measured by GC-IRMS ($\delta^{13}C_{tot}$) for the two conservative hypotheses: (1) a difference between the carbon isotope signature of the spiked METO and the METO-d6 used as a surrogate of +10‰ (blue line), and (2) a difference of -10‰ (orange line).

Table S7 shows the selection of samples for δ^{13}C-METO determinations, following the <5% METO-d6 criteria and based on the known mass of metolachlor and metolachlor-d6 in each soil extract. The offset between the measured δ_{tot} and the expected δ_{meto} is within measurement uncertainty (±0.5‰) for all selected samples, based on the two conservative hypotheses for the isotope signature of METO-d6 of ±10‰ compared to the δ^{13}C of the spiked METO.

Table S7. Offset between the measured $\delta^{13}C_{total}$ and the expected $\delta^{13}C_{meto}$ for the selected extracts for carbon isotope measurements, following the two conservative hypotheses of ±10‰ deviation of the isotope signature of METO-d6 compared to the δ^{13}C of the spiked METO.

						Hypothesis 1 Deviation of +10‰		**Hypothesis 2 Deviation of -10‰**	
Samples	**METO (µg)**	**METO-d6 (µg)**	**Total (µg)**	**% METO-d6**	**Measured δ_{tot} (‰)**	**Estimated $\delta^{13}C_{meto}$ (‰)**	**Offset (‰)**	**Estimated $\delta^{13}C_{meto}$ (‰)**	**Offset (‰)**
M1	40.2	0.7	40.9	1.7	-30.0	-30.2	0.2	-29.9	-0.1
M2	42.1	0.6	42.7	1.5	-29.8	-30.0	0.2	-29.7	-0.1
M3	27.2	0.4	27.6	1.5	-29.6	-29.8	0.2	-29.5	-0.1
M4	29.7	0.5	30.2	1.7	-29.0	-29.2	0.2	-28.8	-0.2
M5	24.0	0.6	24.6	2.5	-28.9	-29.2	0.3	-28.6	-0.3
M6	18.5	0.9	19.4	4.5	-27.9	-28.3	0.4	-27.4	-0.5
V1	42.2	0.6	42.8	1.5	-30.5	-30.7	0.2	-30.4	-0.1
V2	37.7	0.6	38.3	1.6	-30.1	-30.3	0.2	-30.0	-0.1
V3	19.4	0.6	20.0	3.0	-28.7	-29.0	0.3	-28.4	-0.3
V5	23.4	0.5	23.9	2.2	-28.4	-28.6	0.2	-28.2	-0.2
V6	26.6	0.6	27.1	2.1	-28.3	-28.5	0.2	-28.1	-0.2
V7	18.0	0.8	18.8	4.2	-27.5	-27.9	0.4	-27.0	-0.5

6. Chloroacetanilides hydrolysis

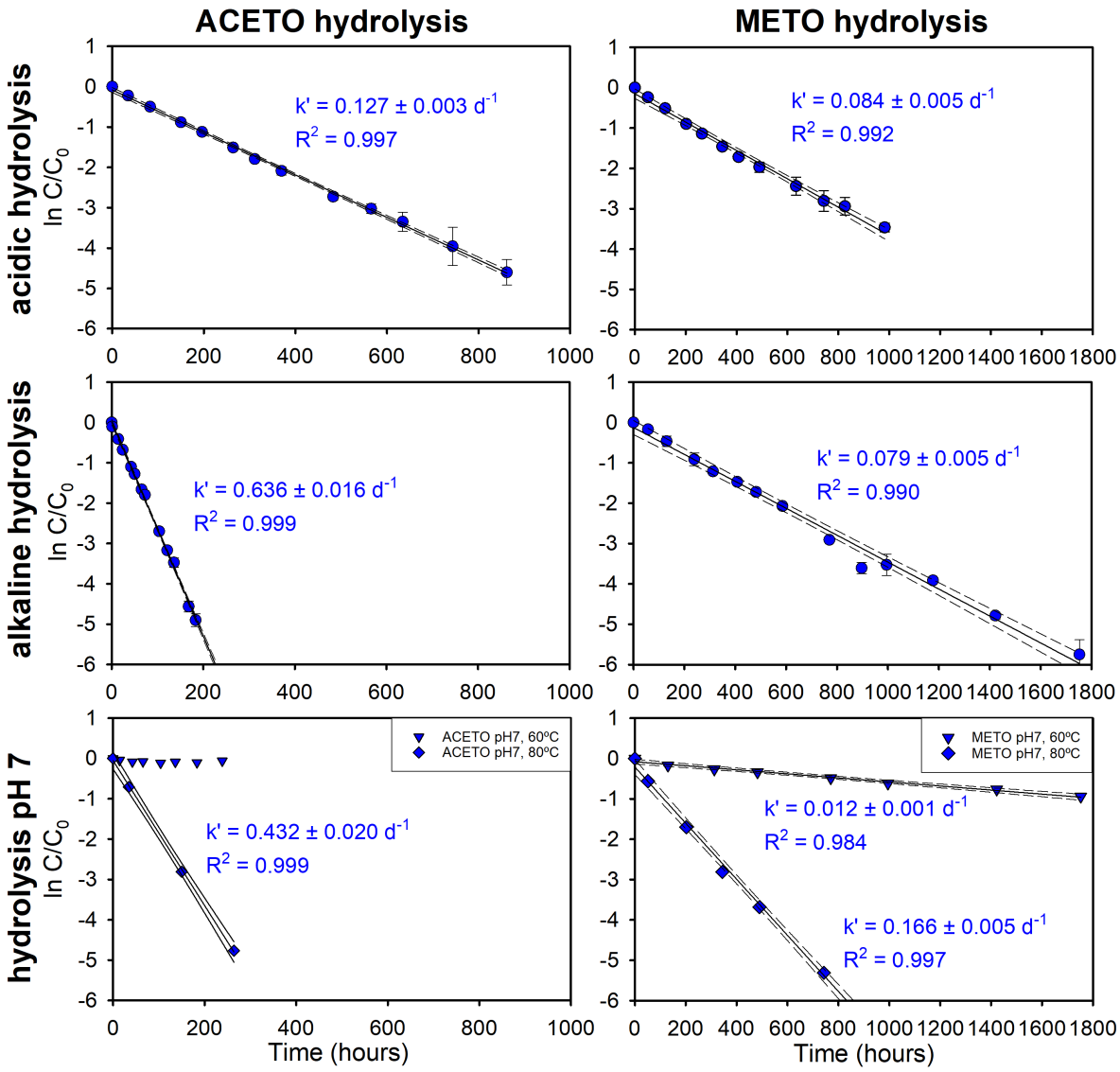

Figure S3. Semi-logarithmic plot of kinetics of ACETO and METO degradation by acidic (pH 3 at 80°C, upper panels), alkaline (pH 12 at 60°C, middle panels) and neutral (pH 7 at both 60°C and 80°C, lower panels) hydrolysis. Averaged data from the triplicate experiments are shown. Error bars stand for the standard deviation of these triplicate experiments. Pseudo-first-order rate constants (k') were extracted from curve fittings according to **Eq. S1**. Dashed lines represent 95% CI of linear regression. Regression lines are only shown when $p<0.05$.

Table S8. Kinetics of acidic, neutral and alkaline hydrolysis of ACETO and METO, and comparison with previous studies. Pseudo-first order constant rates (k', **Eq. S1**), half-lives ($t_{1/2}$, **Eq. S2**) and detected degradation products are shown, as well as experimental conditions. Details about the non-hydroxylated degradation products found in this study (products **I**, **II**, **III, IV** and **V**) are shown in **Figure S4**. *denotes a putative structure.

Acetochlor (abiotic hydrolysis)

Hydrolysis conditions	pH	T. (°C)	k' (d^{-1}) ± 95%CI	$t_{1/2}$ (d) ± 95%CI	Degradation products	Reference
Acidic	-0.3	25	$2.3 \times 10^{-1} \pm 1.6 \times 10^{-2}$	2.9 ± 0.2	CMEPA	Carlson et al. (2006)
Acidic	2	20 & 30	No degradation ($t_{1/2}$ > 200 days, p > 0.05)			Masbou et al. (2018)
Acidic	3	80	$1.3 \times 10^{-1} \pm 3.2 \times 10^{-3}$	5.4 ± 0.1	HACETO, CMEPA (**I**)*, N-(2-ethyl-6-methylphenyl)-2-hydroxyacetamide (**II**)*	**This study**
Acidic	4	20 & 30	No degradation ($t_{1/2}$ > 200 days, p > 0.05)			Masbou et al. (2018)
Neutral	7	20 & 30	No degradation ($t_{1/2}$ > 200 days, p > 0.05)			Masbou et al. (2018)
Neutral	7	60	No degradation (p > 0.05)			**This study**
Neutral	7	80	$4.3 \times 10^{-1} \pm 1.2 \times 10^{-2}$	1.6 ± 0.1	HACETO	**This study**
Alkaline	9	20 & 30	No degradation ($t_{1/2}$ > 200 days, p > 0.05)			Masbou et al. (2018)
Alkaline	12	20	$9.0 \times 10^{-3} \pm 2.0 \times 10^{-3}$	75 ± 17	HACETO	Masbou et al. (2018)
Alkaline	12	30	$3.8 \times 10^{-2} \pm 3.0 \times 10^{-3}$	18 ± 2	HACETO	Masbou et al. (2018)
Alkaline	12	60	$6.4 \times 10^{-1} \pm 1.6 \times 10^{-2}$	1.1 ± 0.03	HACETO, N-(2-ethyl-6-methylphenyl)-2-hydroxyacetamide (**II**)*, N-(ethoxymethyl)-N-(2-ethyl-6-methylphenyl)-2-methoxyacetamide (**III**)*	**This study**
Alkaline	14.3	25	2.6 ± 0.08	0.26 ± 0.01	HACETO	Carlson et al. (2006)

Metolachlor (abiotic hydrolysis)

Hydrolysis conditions	pH	T. (°C)	k' (d^{-1}) ± 95%CI	$t_{1/2}$ (d) ± 95%CI	Degradation products	Reference
Acidic	-0.9	58	$2.4 \times 10^{-1} \pm 1.6 \times 10^{-2}$	0.04 ± 0.001	Metolachlor-desmethyl, Metolachlor morpholinone	Arcelli et al. (1997)
Acidic	-0.3	85	63 ± 3	0.01± 0.001	Metolachlor-desmethyl, Metolachlor morpholinone, amino alcohol, 2-ethyl-6-methylaniline, aminoester, CMEPA	Carlson et al. (2006)
Acidic	-0.3	25	7.8×10^{-4} – 1.7×10^{-3}	401 – 891	No degradation products identified	Carlson et al. (2006)
Acidic	1	30-50-70	-	>200 d at 20°C	Metolachlor-desmethyl, Metolachlor morpholinone	LeBaron et al. (1988)
Acidic	2	20 & 30	No degradation ($t_{1/2}$ > 200 days, p > 0.05)			Masbou et al. (2018)
Acidic	2	38	No degradation (less than 5% after 50 days)			Ripley et al. (1986)

Acidic	3	80	$8.4 \times 10^{-2} \pm 5.3 \times 10^{-3}$	8.3 ± 0.5	HMETO, 4-(2-Ethyl-6-methylphenyl)-5-methyl-3-morpholinone (Metolachlor-morpholinone) (**IV**)*	**This study**
Neutral	7	20 & 30	No degradation ($t_{1/2}$ > 200 days, p > 0.05)			Masbou et al. (2018)
Neutral	7	20	No degradation (less than 5% after 100 days)			Kochany et al. (1994)
Neutral	7	60	$1.2 \times 10^{-2} \pm 1.4 \times 10^{-3}$	58 ± 7	HMETO, 4-(2-Ethyl-6-methylphenyl)-5-methyl-3-morpholinone (Metolachlor-morpholinone) (**IV**)*	**This study**
Neutral	7	80	$1.7 \times 10^{-1} \pm 5.2 \times 10^{-3}$	4.2 ± 0.1	HMETO, 4-(2-Ethyl-6-methylphenyl)-5-methyl-3-morpholinone (Metolachlor-morpholinone) (**IV**)*	**This study**
Alkaline	12	20 & 30	No degradation ($t_{1/2}$ > 200 days, p > 0.05)			Masbou et al. (2018)
Alkaline	12	20	No degradation ($t_{1/2}$ > 200 days, p > 0.05)			Masbou et al. (2018)
Alkaline	12	30	$6.0 \times 10^{-3} \pm 1.0 \times 10^{-3}$	122 ± 26	No degradation products identified	Masbou et al. (2018)
Alkaline	12	60	$7.9 \times 10^{-2} \pm 5.0 \times 10^{-3}$	8.8 ± 0.6	HMETO, 4-(2-Ethyl-6-methylphenyl)-5-methyl-3-morpholinone (Metolachlor-morpholinone) (**IV**)*, N-(2-ethyl-6-methylphenyl)-2-methoxy-N-(1-methoxypropan-2-yl)acetamide (**V**)*	**This study**
Alkaline	13	20	7.2×10^{-3}	97	HMETO	LeBaron et al. (1988)
Alkaline	14.3	25	$3.3 \times 10^{-1} \pm 1.0 \times 10^{-2}$	2.1 ± 0.1	HMETO	Carlson et al. (2006)

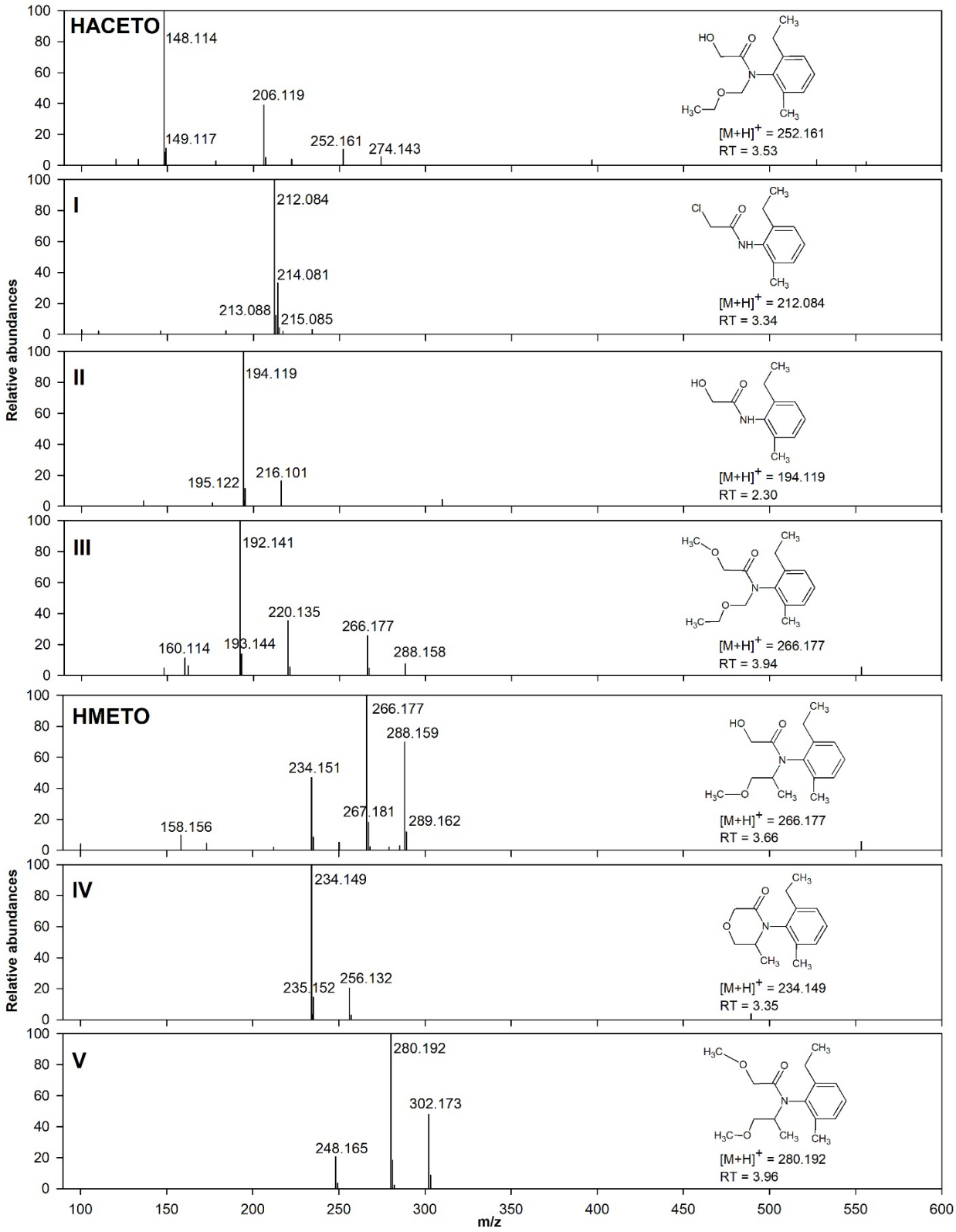

Figure S4. Mass spectra of the degradation products found in the ACETO and METO hydrolysis experiments. Tentatively assigned structures are also shown. Identification of HACETO and HMETO was corroborated by mass spectra and retention time matching the authentic standards. Tentative identification occurred when an expected ion was found with mass error below 5 ppm, together with its characteristic isotopic pattern (if present), and one or more fragment ions were in agreement with data reported and compatible with the chemical structure of the candidate.

HACETO. The signals at *m/z* 252.161 and 274.143 correspond to the protonated molecule ($C_{14}H_{22}NO_3^+$) and its sodium adduct, respectively. The most abundant fragment ions are observed at *m/z* 148.114 ($C_{10}H_{14}N^+$, from $C_4H_8O_3$ loss) and 206.119 ($C_{12}H_{16}NO_2^+$, from C_2H_5OH loss).

I, 2-Chloro-N-(2-ethyl-6-methylphenyl)acetamide (CMEPA). The signal at *m/z* 212.084 might correspond to the protonated molecule ($C_{11}H_{15}ClNO^+$).

II, N-(2-ethyl-6-methylphenyl)-2-hydroxy acetamide. The signals at *m/z* 194.119 and 216.111 might correspond to the protonated molecule ($C_{11}H_{16}NO_2^+$) and its sodium adduct, respectively.

III, N-(ethoxymethyl)-N-(2-ethyl-6-methylphenyl)-2-methoxyacetamide. The signal at *m/z* 266.177 might correspond to the protonated molecule ($C_{15}H_{24}NO_3^+$). The most abundant fragment ions are observed at *m/z* 192.141 ($C_{12}H_{18}NO^+$, from $C_3H_6O_2$ loss) and 220.135 ($C_{13}H_{18}NO_2^+$, from C_2H_5OH loss).

HMETO. The signals at *m/z* 266.177 and 288.159 correspond to the protonated molecule ($C_{15}H_{24}NO_3^+$) and its sodium adduct, respectively. One fragment ion is also observed at *m/z* 234.151 ($C_{14}H_{21}NO_2^+$, from CH_3O loss).

IV, N-(2-ethyl-6-methylphenyl)-2-hydroxyacetamide (Metolachlor-morpholinone). The signals at *m/z* 234.149 and 256.132 might correspond to the protonated molecule ($C_{14}H_{20}NO_2^+$) and its sodium adduct, respectively.

V, N-(2-ethyl-6-methylphenyl)-2-methoxy-N-(1-methoxypropan-2-yl)acetamide. The signal at *m/z* 280.192 might correspond to the protonated molecule ($C_{16}H_{26}NO_3^+$). One fragment ion is also observed at *m/z* 248.165 ($C_{15}H_{22}NO_2^+$, from CH_3OH loss).

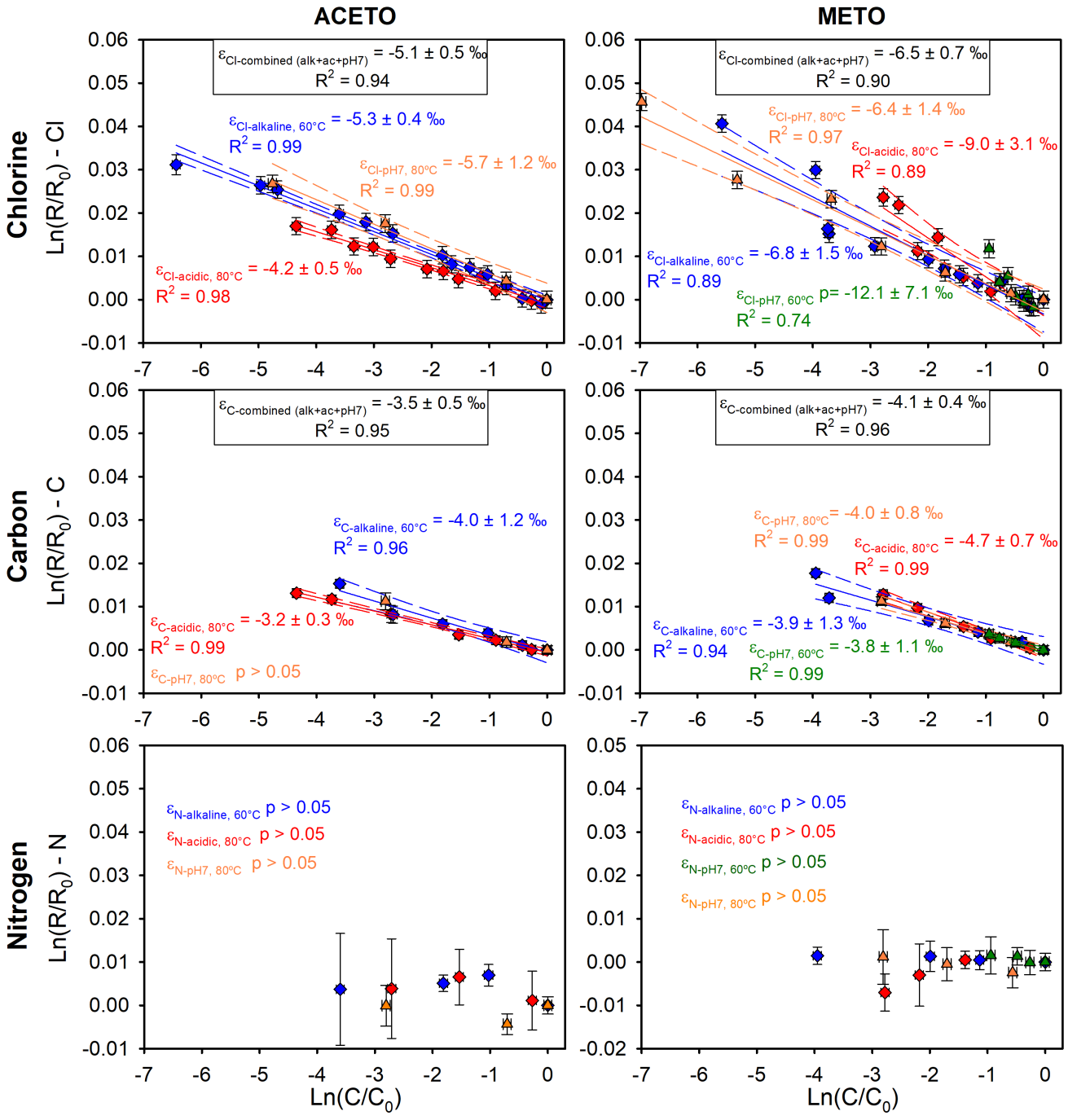

Figure S5. Logarithmic plots according to Rayleigh equation (**Eq. 2**) for Cl (upper panels), C (middle panels) and N (lower panels) fractionation during ACETO (left panels) and METO (right panels) hydrolysis. Red symbols stand for acidic hydrolysis (pH 3 at 80°C), blue symbols for alkaline hydrolysis (pH 12 at 60°C), green symbols for experiments at pH 7 and 60°C and orange symbols for experiments at pH 7 and 80°C. Error bars display the uncertainty calculated by error propagation including uncertainties in concentration and isotope measurements. Solid lines represent OLR fits with 95% CI (dashed lines). Regression lines are only shown when $p<0.05$. When differences between the regressed data from the different experimental conditions were not significant ($p>0.05$), data were merged to derive combined ε values.

Table S9. Isotopic results for ACETO and METO abiotic hydrolysis experiments under acidic, neutral and alkaline conditions. Carbon, nitrogen and chlorine isotope fractionation (ε_C, ε_N, ε_{Cl}) and apparent kinetic isotope effect ($AKIE_C$, $AKIE_N$, $AKIE_{Cl}$) values are shown, as well as 2D-isotope slopes ($\Lambda_{N/C}$, $\Lambda_{C/Cl}$ and $\Lambda_{N/Cl}$). Comparison with previous studies is also shown. The uncertainty is shown as the 95% confidence interval (95% CI). Λ values were obtained by ordinary linear regression. 2D-isotope slopes previously reported for other transformation reactions are also shown. Available data for each transformation reaction were merged to obtain combined $\Lambda_{N/C}$, $\Lambda_{C/Cl}$ and $\Lambda_{N/Cl}$ values, when possible. n.a = not analyzed; n.s = not significant.

Acetochlor

	ε_C (‰) ± 95% CI	ε_N (‰) ± 95% CI	ε_{Cl} (‰) ± 95% CI	$AKIE_C$ ± 95% CI	$AKIE_N$ ± 95% CI	$AKIE_{Cl}$ ± 95% CI	Reference
pH 3 (80°C)	-3.2±0.3	n.s	-4.2±0.5	1.047±0.005	-	1.004±0.0005	**This study**
pH 7 (80°C)	n.s	n.s	-5.7±1.2	n.s	-	1.006±0.001	**This study**
pH 12 (20&30°C)	-4.0±0.8	n.s	n.a	1.060±0.012	-	n.a	Masbou et al. (2018)
pH 12 (60°C)	-4.0±1.2	n.s	-5.3±0.4	1.059±0.019	-	1.005±0.0004	**This study**

	$\Lambda_{N/C}$ ± 95% CI	$\Lambda_{C/Cl}$ ± 95% CI	$\Lambda_{N/Cl}$ ± 95% CI	Reference
pH 3 (80°C)	n.s	0.72±0.08	n.s	**This study**
pH 7 (80°C)	n.s	n.s	n.s	**This study**
pH 12 (20&30°C)	n.s	n.a	n.a	Masbou et al. (2018)
pH 12 (60°C)	n.s	0.65±0.24	n.s	**This study**
Acidic + neutral + alkaline hydrolysis	*n.s*	*0.67±0.08*	*n.s*	*combined data*

Metolachlor

	ε_C (‰) ± 95% CI	ε_N (‰) ± 95% CI	ε_{Cl} (‰) ± 95% CI	$AKIE_C$ ± 95% CI	$AKIE_N$ ± 95% CI	$AKIE_{Cl}$ ± 95% CI	Reference
pH 3 (80°C)	-4.7±0.7	n.s	-9.0±3.1	1.076±0.013	-	1.009±0.003	**This study**
pH 7 (60°C)	-3.8±1.1	n.s	-12.1±7.1	1.060±0.019	-	1.012±0.007	**This study**
pH 7 (80°C)	-4.0±0.8	n.s	-6.4±1.4	1.063±0.010	-	1.006±0.001	**This study**
pH 12 (30°C)	-2.8±0.6	-2.0±1.3	n.a	1.043±0.008	1.002±0.001	n.a	Masbou et al. (2018)
pH 12 (60°C)	-3.9±1.3	n.s	-6.8±1.5	1.062±0.022	-	1.007±0.002	**This study**

	$\Lambda_{N/C}$ ± 95% CI	$\Lambda_{C/Cl}$ ± 95% CI	$\Lambda_{N/Cl}$ ± 95% CI	Reference
pH 3 (80°C)	n.s	0.51±0.20	-0.32±0.28	**This study**
Acidic hydrolysis	*n.s*	*0.51±0.20*	*-0.32±0.28*	*combined data*
pH 7 (60°C)	n.s	n.s	n.s	**This study**
pH 7 (80°C)	n.s	0.87±0.16	n.s	**This study**
Neutral hydrolysis	*n.s*	*0.87±0.16*	*n.s*	*combined data*
pH 12 (30°C)	0.79±0.71	n.a	n.a	Masbou et al. (2018)
pH 12 (60°C)	n.s	0.55±0.13	n.s	**This study**
Alkaline hydrolysis	*0.79±0.71*	*0.55±0.13*	*n.s*	*combined data*

7. Comparison between OLR and York regression methods for estimating 2D-CSIA slopes

A recent study by Ojeda et al. (2019) suggested to use the York regression method instead of OLR to determine Λ and its uncertainty. Indeed, the OLR approach does not take into account the error in the x- variable while the York method uses error both in the x and y variables. According to Ojeda at al. (2019), C-Cl dual isotope plots would be more susceptible to slope attenuation (*i.e.*, a slope closer to zero) introduced by OLR because the analytical uncertainty for C and Cl measurements is comparable, and ignoring the error in the x- variable would lead to a stronger slope attenuation and to an artificially smaller SE associated to OLR. A comparison between lambda values and their uncertainties obtained in this study with the York and the OLR regression methods is shown in **Table S10**. For OLR, slope attenuation is observed for $\Lambda_{C/Cl}$ for hydrolysis of the three studied compounds at pH 3 and for METO degradation in soil M, as predicted by Ojeda et al. (2019), but not for $\Lambda_{C/Cl}$ for METO hydrolysis at pH 12 and pH 7, for which OLR and the York method give identical slopes. Since no systematic bias introduced by OLR was observed for $\Lambda_{C/Cl}$ and SE was generally higher for OLR than for the York method, we therefore decided to use OLR.

Table S10. 2D-isotope slopes ($\Lambda_{N/C}$, $\Lambda_{C/Cl}$ and $\Lambda_{N/Cl}$) for acidic, neutral and alkaline hydrolysis of ACETO, METO and ATR and for METO degradation in soil, obtained by OLR or by the York regression method. SE = standard error, n = number of points, 95% CI = 95% confidence interval. n.s = not significant. n.a = not analyzed.

Acetochlor

		$\Lambda_{N/C}$	SE	n	95% CI	$\Lambda_{C/Cl}$	SE	n	95% CI	$\Lambda_{N/Cl}$	SE	n	95% CI
pH 3 (80°C)	**Linear regression**	n.s				0.72	0.03	7	0.08	n.s			
	York method					0.76	0.03	7	0.08				
pH 12 (60°C)	**Linear regression**	n.s				0.65	0.09	6	0.24	n.s			
	York method	0.98	0.18	4	0.77	0.69	0.03	6	0.09	0.57	0.09	4	0.40
pH 7 (80°C)	**Linear regression**	n.s				n.s				n.s			
	York method												

Metolachlor hydrolysis

		$\Lambda_{N/C}$	SE	n	95% C	$\Lambda_{C/Cl}$	SE	n	95% CI	$\Lambda_{N/Cl}$	SE	N	95% CI
pH 3 (80°C)	**Linear regression**	n.s				0.51	0.07	6	0.20	-0.32	0.06	4	0.28
	York method	n.s				0.60	0.02	6	0.06	n.s			
pH 12 (60°C)	**Linear regression**	n.s				0.55	0.05	6	0.13	n.s			
	York method	n.s				0.55	0.02	6	0.06	n.s			
pH 7 (60°C)	**Linear regression**	n.s				n.s				n.s			
	York method					0.26	0.05	4	0.24				
pH 7 (80°C)	**Linear regression**	n.s				0.87	0.04	4	0.16	n.s			
	York method					0.87	0.04	4	0.18				

Metolachlor soil degradation

		$\Lambda_{N/C}$	SE	n	95% CI	$\Lambda_{C/Cl}$	SE	n	95% CI	$\Lambda_{N/Cl}$	SE	N	95% CI
Soil M	**Linear regression**	n.a				0.51	0.10	6	0.28	n.a			
	York method	n.a				0.50	0.14	6	0.40	n.a			
Soil V	**Linear regression**	n.a				n.s				n.a			

York method	n.a				0.42	0.30	5	0.97	n.a			

Atrazine

		$\Lambda_{N/C}$	SE	n	95% CI	$\Lambda_{C/Cl}$	SE	n	95% CI	$\Lambda_{N/Cl}$	SE	n	95% CI
pH 3 (25°C)	**Linear regression**	-0.61	0.03	6	0.08	8.3	0.6	7	1.5	-4.8	0.6	6	1.7
	York method	-0.60	0.02	6	0.07	8.5	1.2	7	3.0	-5.1	1.0	6	2.8
pH 12 (25°C)	**Linear regression**	0.32	0.05	5	0.17			n.s				n.s	
	York method	0.28	0.03	5	0.11	7.0	1.8	5	5.6	1.8	0.5	5	1.6

8. Biodegradation of metolachlor in the two soils

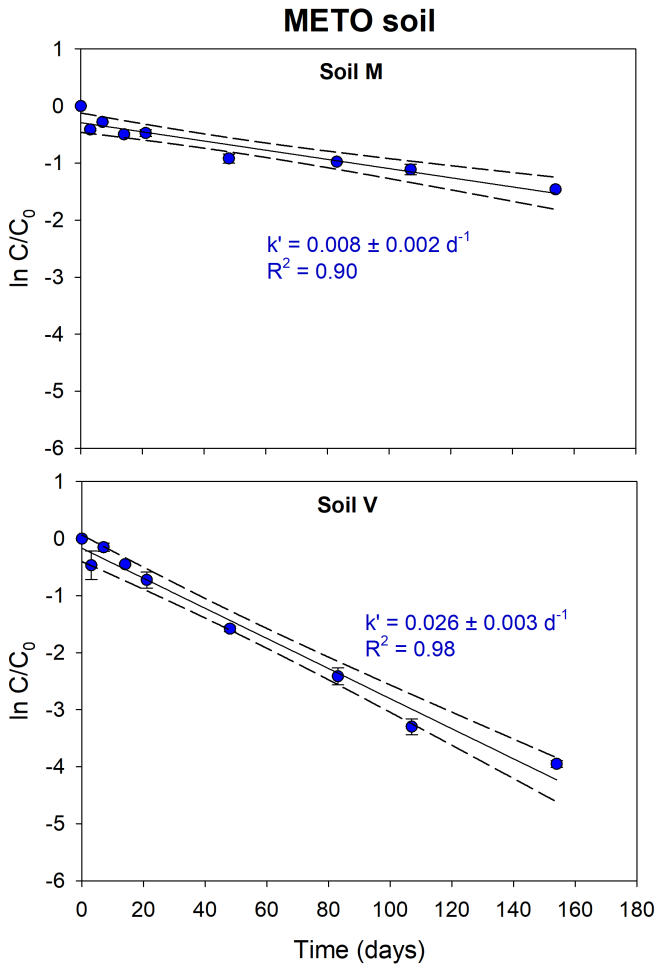

Figure S6. Semi-logarithmic plot of kinetics of METO degradation in experiments with soil M (upper panel), and soil V (lower panel). Averaged data from the duplicate experiments are shown. Error bars stand for the standard deviation of these duplicate experiments. Pseudo-first-order rate constants (k') were extracted from curve fittings according to **Eq. S1**. Dashed lines represent 95% CI of linear regression.

Table S11. Kinetics of METO degradation in the two soils. Pseudo-first order constant rates (k', **Eq. S1**), half-lives ($t_{1/2}$, **Eq. S2**) and detected degradation products are shown, as well as experimental conditions.

Soil	T. (°C)	Water content (%)	k' (d^{-1}) ± 95%CI	$t_{1/2}$ (d) ± 95%CI	Degradation products	Reference
M	25	15	8.0×10^{-3} ± 2.4×10^{-3}	86 ± 26	Metolachlor ESA; metolachlor OXA	**This study**
V	25	15	2.6×10^{-2} ± 3.3×10^{-3}	26 ± 3	Metolachlor ESA; metolachlor OXA	**This study**

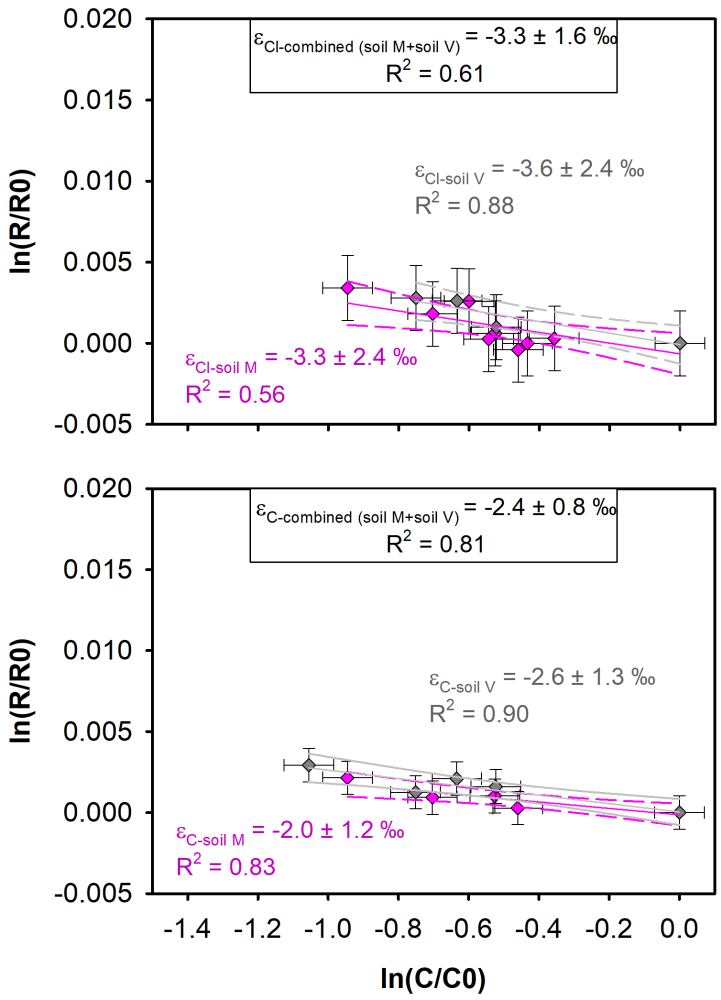

Figure S7. Logarithmic plots according to Rayleigh equation (**Eq. 2**) for Cl (upper panel) and C (lower panel) fractionation during METO degradation in soils. Gray symbols stand for degradation in soil M and pink symbols for soil V. Error bars display the uncertainty calculated by error propagation including uncertainties in concentration and isotope measurements. Solid lines represent OLR fits with 95% CI (dashed lines). Regression lines are only shown when $p<0.05$. When differences between the results of the different experimental conditions were not significant ($p>0.05$), data were merged to derive combined ε values.

Table S12. Isotopic results for METO degradation in soils from different studies, including this one. Carbon, nitrogen and chlorine isotope fractionation (ε_C, ε_N, ε_{Cl}) and apparent kinetic isotope effect ($AKIE_C$, $AKIE_N$, $AKIE_{Cl}$) values are shown, as well as 2D-isotope slopes ($\Lambda_{N/C}$, $\Lambda_{C/Cl}$ and $\Lambda_{N/Cl}$). The uncertainty is shown as the 95% confidence interval (95% CI). Λ values were obtained by ordinary linear regression. 2D-isotope slopes previously reported for other transformation reactions are also shown. Available data for each transformation reaction were merged to obtain combined $\Lambda_{N/C}$, $\Lambda_{C/Cl}$ and $\Lambda_{N/Cl}$ values, when possible. n.a = not analyzed, n.s = not significant.

	ε_C (‰) ± 95% CI	**ε_N (‰) ± 95% CI**	**ε_{Cl} (‰) ± 95% CI**	**$AKIE_C$ ± 95% CI**	**$AKIE_N$ ± 95% CI**	**$AKIE_{Cl}$ ± 95% CI**	**Reference**
Soil M	-2.0±1.2	n.a	-3.3±2.4	1.031±0.020	n.a	1.003±0.002	**This study**
Soil V	-2.6±1.3	n.a	-3.6±2.4	1.040±0.021	n.a	1.004±0.002	**This study**
Alteckendorf crop soil	-1.5±0.5	inverse, high uncertainty	n.a	1.023±0.007	n.a	n.a	Alvarez-Zaldívar et al. (2018)
Bas Rhin crop soil	-1.4±0.3 to -1.8±0.3	n.a	n.a	1.021±0.004 to 1.028±0.004	n.a	n.a	Meite (2018)
Rouffach wetland sediment	-1.2±0.2	n.s ($\lvert\Delta\delta^{15}N\rvert$ < 2‰)	n.a	1.018±0.001	n.s	n.a	Droz et al. (2021)
Rouffach wetland sediment (anoxic)	-1.8±0.3	n.s ($\lvert\Delta\delta^{15}N\rvert$ < 2‰)	n.a	1.018±0.001	n.s	n.a	Droz et al. (2021)

	$\Lambda_{N/C}$ ± 95% CI	**$\Lambda_{C/Cl}$ ± 95% CI**	**$\Lambda_{N/Cl}$ ± 95% CI**	**Reference**
Soil M	n.a	0.51±0.28	n.a	**This study**
Soil V	n.a	n.s	n.a	**This study**
Rouffach vineyard soil (planted)	0.7±0.6	n.a	n.a	Pérez-Rodríguez et al. (2021)
Rouffach vineyard soil (unplanted)	1.8±0.8	n.a	n.a	Pérez-Rodríguez et al. (2021)
Soil degradation	-	*0.53±0.22*	*n.a*	*combined data*

9. Hydrolysis of atrazine

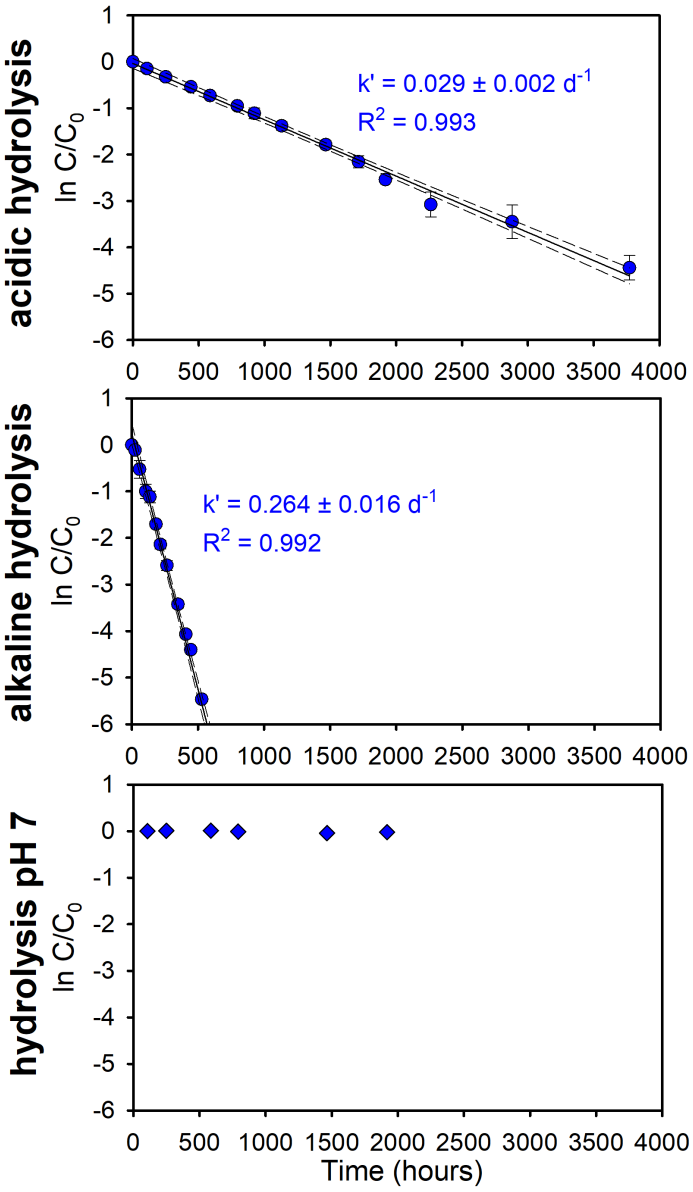

Figure S8. Semi-logarithmic plot of kinetics of ATR degradation by acidic (pH 3, upper panel), alkaline (pH 12, middle panel) and neutral (pH 7, lower panel) hydrolysis at 25°C. Averaged data from the triplicate experiments are shown. Error bars stand for the standard deviation of these triplicate experiments. Pseudo-first-order rate constants (k') were extracted from curve fittings according to **Eq. S1**. Dashed lines represent 95% CI of linear regression. Regression lines are only shown when $p<0.05$.

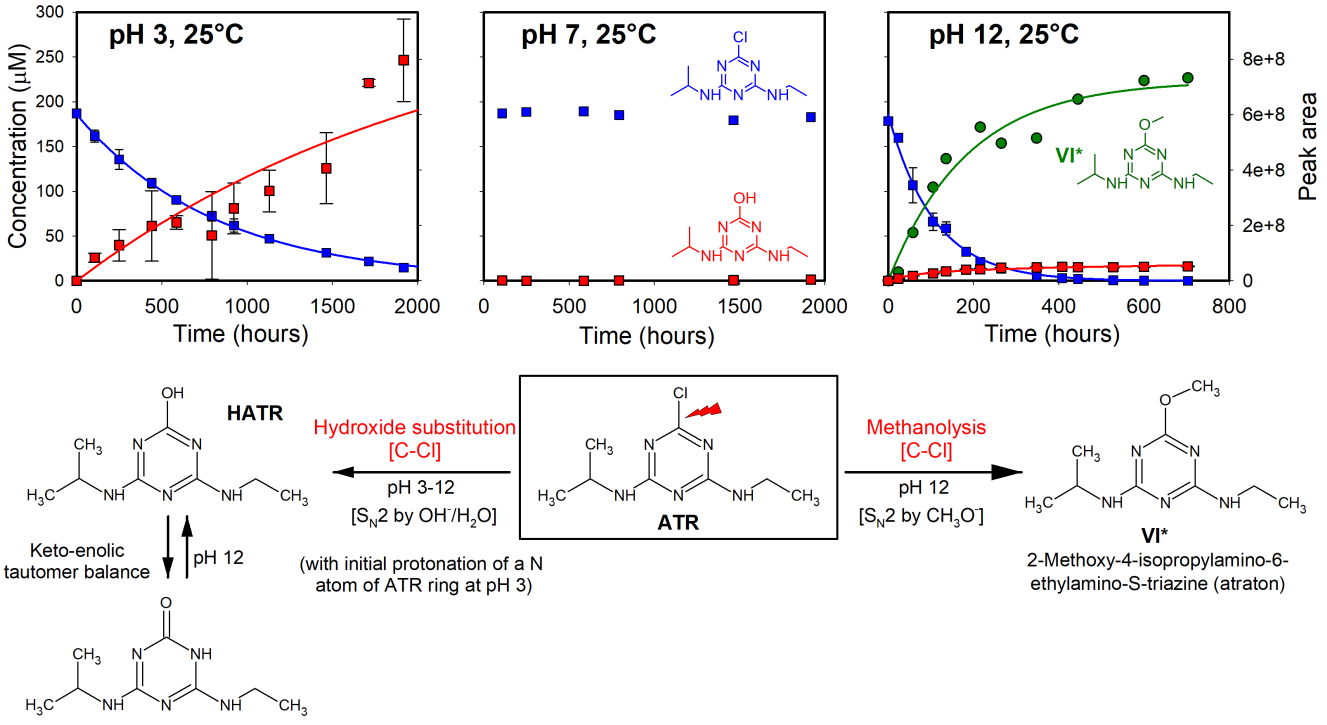

Figure S9. Time courses and postulated possible degradation pathways for acidic, neutral and alkaline hydrolysis of ATR at 25°C. Concentration of ATR (blue squares) and the hydroxylated product HATR (red squares) is shown for triplicate experiments. Error bars stand for the standard deviation of concentrations in triplicate experiments. The peak areas obtained by UHPLC-QTOF-MS are shown for the non-hydroxylated transformation product **VI** (green circles). Solid lines represent model fits assuming pseudo-first-order transformation. * denotes a putative structure.

Table S13. Kinetics of acidic, neutral and alkaline hydrolysis of ATR, and comparison with previous studies. Pseudo-first order constant rates (k', **Eq. S1**), half-lives ($t_{1/2}$, **Eq. S2**) and detected degradation products are shown, as well as experimental conditions. Details about the non-hydroxylated degradation product found in this study (product **VI**) are shown in **Figure S10**. *denotes a putative structure.

Hydrolysis conditions	pH	T. (°C)	k' (d^{-1}) ± 95%CI	$t_{1/2}$ (d) ± 95%CI	Degradation products	Reference
Acidic	0.5 – 0.7	25	2.4×10^{-1} – 4.0×10^{-1}	1.7 – 2.9	Not reported	Plust et al. (1981)
Acidic	0.4 – 0.9	40	1.0 – 1.7	0.4 – 0.7	Not reported	Plust et al. (1981)
Acidic	1.1 – 2.1	25	1.4×10^{-1} – 4.3×10^{-2}	5.0 – 16.1	Not reported	Plust et al. (1981)
Acidic	1.0 – 1.6	40	3.1×10^{-1} – 8.6×10^{-1}	0.8 – 2.2	Not reported	Plust et al. (1981)
Acidic	2	20	$1.3 \times 10^{-2} \pm 1.0 \times 10^{-3}$	53 ± 6	HATR	Masbou et al. (2018)
Acidic	2	30	$7.0 \times 10^{-2} \pm 1.0 \times 10^{-2}$	9.7 ± 1.4	HATR	Masbou et al. (2018)
Acidic	3	25	$2.9 \times 10^{-2} \pm 1.5 \times 10^{-3}$	24 ± 1	HATR, atraton (**VI**)*	**This study**
Acidic	3.1	40	2.2×10^{-2}	31	Not reported	Plust et al. (1981)
Acidic	3	60	$9.1 \times 10^{-2} \pm 6.0 \times 10^{-3}$	7.6 ± 0.5	HATR	Meyer et al. (2009)
Acidic	4	20	$9.0 \times 10^{-3} \pm 2.0 \times 10^{-3}$	78 ± 19	HATR	Masbou et al. (2018)
Acidic	4	30	$1.6 \times 10^{-2} \pm 4.0 \times 10^{-3}$	43 ± 10	HATR	Masbou et al. (2018)
Acidic	4	40	1.4×10^{-2}	49	Not reported	Plust et al. (1981)
Neutral	7	20 & 30	No degradation ($t_{1/2}$ > 200 days, p > 0.05)			Masbou et al. (2018)
Neutral	7	25	No degradation (p > 0.05)			**This study**
Alkaline	11.1	25	8.5×10^{-3}	81	Not reported	Plust et al. (1981)
Alkaline	12	Not reported	1.0×10^{-2}	69	HATR	Prosen and Zupancic-Kralj (2005)
Alkaline	11.9	25	4.6×10^{-2}	15	Not reported	Plust et al. (1981)
Alkaline	12	20	$2.2 \times 10^{-2} \pm 7.2 \times 10^{-4}$	32 ± 1	HATR	Meyer et al. (2009)
Alkaline	12	20	$3.3 \times 10^{-2} \pm 5.0 \times 10^{-3}$	21 ± 3	HATR	Masbou et al. (2018)
Alkaline	12	25	$2.6 \times 10^{-1} \pm 1.6 \times 10^{-2}$	2.6 ± 0.2	HATR	**This study**
Alkaline	12	30	$1.2 \times 10^{-1} \pm 1.0 \times 10^{-2}$	5.9 ± 0.6	HATR	Masbou et al. (2018)
Alkaline	12	60	$4.4 \times 10^{-2} \pm 3.3 \times 10^{-3}$	16 ± 1	HATR	Meyer et al. (2009)
Alkaline	12.9	25	3.7×10^{-1}	1.9	Not reported	Plust et al. (1981)

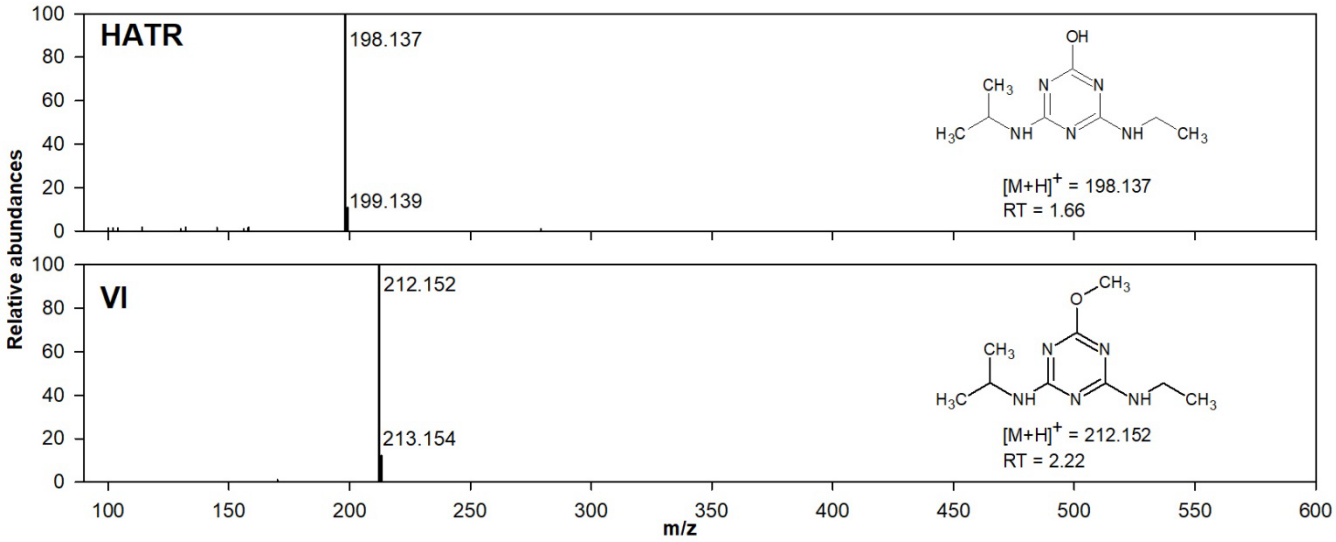

Figure S10. Mass spectra of the degradation products found in the ATR hydrolysis experiments. Tentatively assigned structures are also shown. Identification of HATR was corroborated by mass spectra and retention time matching the authentic standard. Tentative identification occurred when an expected ion was found with mass error below 5 ppm, together with its characteristic isotopic pattern (if present), and one or more fragment ions were in agreement with data previously reported and compatible with the chemical structure of the candidate.

HATR. The signals at *m/z* 198.137 corresponds to the protonated molecule ($C_8H_{16}N_5O^+$).

VI, 2-Methoxy-4-isopropylamino-6-ethylamino-S-triazine (atraton). The signal at *m/z* 212.152 might correspond to the protonated molecule ($C_9H_{18}N_5O^+$).

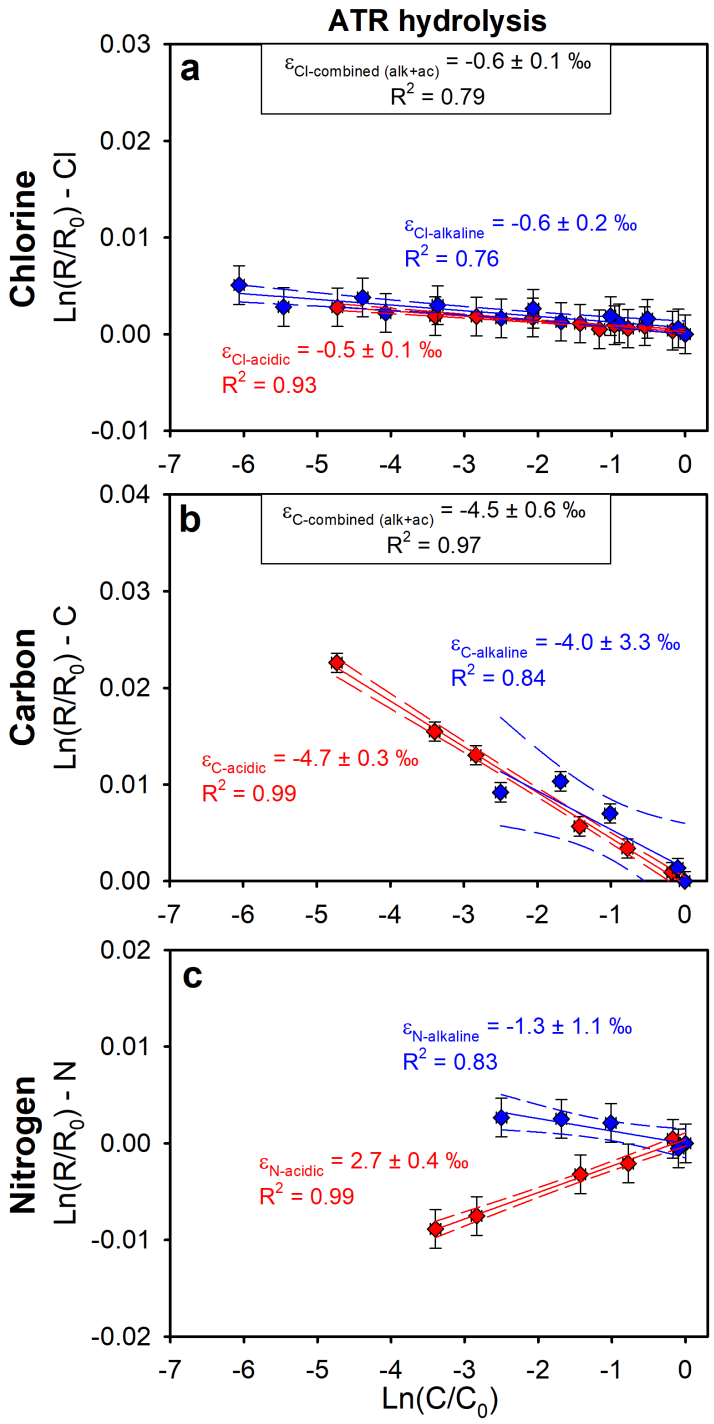

Figure S11. Logarithmic plots according to Rayleigh equation (**Eq. 2**) for Cl (a), C (b) and N (c) fractionation during hydrolysis of ATR at 25°C. Red symbols stand for acidic hydrolysis (pH 3) and blue symbols for alkaline hydrolysis (pH 12). Error bars display the uncertainty calculated by error propagation including uncertainties in concentration and isotope measurements. Solid lines represent OLR fits with 95% CI (dashed lines). When differences between the regressed data from the different experimental conditions were not significant (p>0.05), data were merged to derive combined ε values.

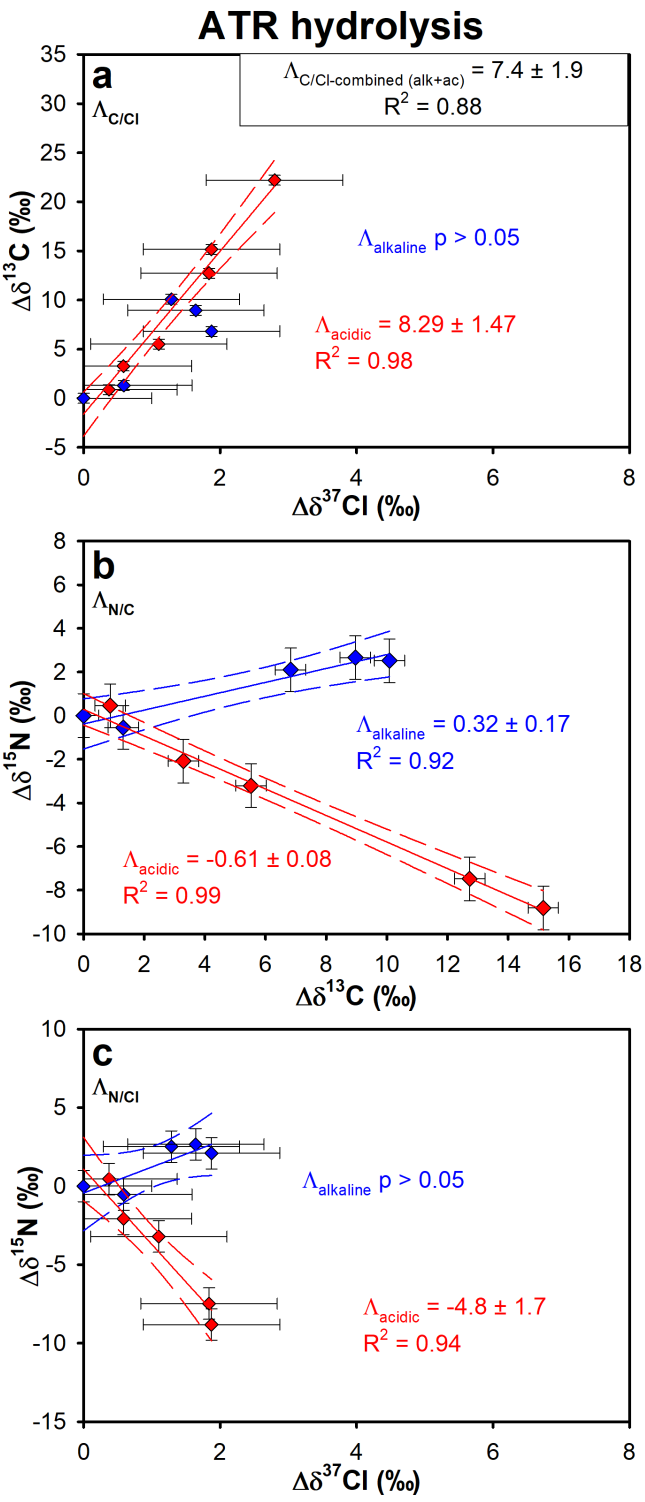

Figure S12. Dual isotope plots for ATR hydrolysis at 25°C under alkaline (pH 12, blue symbols) and acidic (pH 3, red symbols) conditions: $\Delta\delta^{13}C$ vs $\Delta\delta^{37}Cl$ (a), $\Delta\delta^{15}N$ vs $\Delta\delta^{13}C$ (b), and $\Delta\delta^{15}N$ vs $\Delta\delta^{37}Cl$ (c). Error bars display typical uncertainties. Slopes (Λ values) were calculated by OLR and uncertainty is shown as 95% CI. Displayed linear regression are significant except when noted (p>0.05). When differences between the regressed data from the different experimental conditions were not significant (p>0.05), data were merged to derive combined Λ values.

Table S14. Isotopic results for ATR abiotic hydrolysis experiments under acidic, neutral and alkaline conditions. Carbon, nitrogen and chlorine isotope fractionation (ε_C, ε_N, ε_{Cl}) and apparent kinetic isotope effect ($AKIE_C$, $AKIE_N$, $AKIE_{Cl}$) values are shown, as well as 2D-isotope slopes ($\Lambda_{N/C}$, $\Lambda_{C/Cl}$ and $\Lambda_{N/Cl}$). Comparison with previous studies is also shown. The uncertainty is shown as the 95% confidence interval (95% CI). Λ values were obtained by ordinary linear regression. 2D-isotope slopes previously reported for other transformation reactions are also shown. Available data for each transformation reaction were merged to obtain combined $\Lambda_{N/C}$, $\Lambda_{C/Cl}$ and $\Lambda_{N/Cl}$ values, when possible. n.a = not analyzed; n.s = not significant.

	ε_C (‰) ± 95% CI	**ε_N (‰) ± 95% CI**	**ε_{Cl} (‰) ± 95% CI**	**$AKIE_C$ ± 95% CI**	**$AKIE_N$ ± 95% CI**	**$AKIE_{Cl}$ ± 95% CI**	**Reference**
pH 2 (20&30°C)	-6.1±0.8	1.3±0.6	n.a	1.052±0.006	0.994±0.001	n.a	Masbou et al. (2018)
pH 3 (60°C)	-4.8±0.4	2.5±0.2	n.a	1.040±0.003	0.988±0.001	n.a	Meyer et al. (2009)
pH 3 (25°C)	-4.7±0.3	2.7±0.4	-0.54±0.11	1.039±0.003	0.986±0.002	1.0005±0.0001	**This study**
pH 4 (20&30°C)	-6.2±1.4	n.a	n.a	1.052±0.006	n.a	n.a	Masbou et al. (2018)
pH 12 (20&30°C)	-5.6±0.8	-0.8±0.5	n.a	1.047±0.006	1.0008±0.001	n.a	Masbou et al. (2018)
pH 12 (25°C)	-4.0±3.3	-1.3±1.1	-0.59±0.22	1.033±0.028	1.0013±0.005	1.0006±0.0002	**This study**
pH 12 (20°C)	-5.6±0.2	-1.2±0.2	n.a	1.047±0.002	1.0012±0.000	n.a	Meyer et al. (2008)
pH 12 (60°C)	-3.7±0.4	-0.9±0.3	n.a	1.031±0.003	1.0009±0.000	n.a	Meyer et al. (2009)
pH 12 (50°C)	n.a	n.a	-0.9±0.6[a]	n.a	n.a	1.0009±0.0006	Grzybkowska et al. (2014)

[a]calculated from reported $AKIE_{Cl}$ value

	$\Lambda_{N/C}$ ± 95% CI	**$\Lambda_{C/Cl}$ ± 95% CI**	**$\Lambda_{N/Cl}$ ± 95% CI**	**Reference**
pH 2 (20&30°C)	-0.29±0.12	n.a	n.a	Masbou et al. (2018)
pH 3 (60°C)	-0.52±0.04	n.a	n.a	Meyer et al. (2009)
pH 3 (25°C)	-0.61±0.08	8.3±1.5	-4.8±1.7	**This study**
pH 4 (20&30°C)	n.a	n.a	n.a	Masbou et al. (2018)
Acidic hydrolysis	*-0.52±0.07*	*8.3±1.5*	*-4.8±1.7*	*combined data*
pH 12 (20&30°C)	0.15±0.08	n.a	n.a	Masbou et al. (2018)
pH 12 (25°C)	0.32±0.17	n.s	n.s	**This study**
pH 12 (20°C)	0.22±0.02	n.a	n.a	Meyer et al. (2009)
pH 12 (60°C)	0.26±0.06	n.a	n.a	Meyer et al. (2009)
pH 12 (50°C)	n.a	4.1[a]	n.a	Grzybkowska et al. (2014)
Alkaline hydrolysis	*0.19±0.02*	*4.1*	*n.s*	*combined data*
Arthrobacter aurescens TC1	-0.64±0.11	1.7±0.9	-1.2±0.7	Lihl et al. (2020)
Arthrobacter aurescens TC1	-0.61±0.02	n.a	n.a	Meyer et al. (2009)
Arthrobacter aurescens TC1	-0.55±0.15	n.a	n.a	Ehrl et al. (2019)
Arthrobacter aurescens TC1	-0.45±0.13	n.a	n.a	Ehrl et al. (2019)
Pseudomonas sp. ADP	-0.32±0.06	n.a	n.a	Meyer et al. (2009)
Polaromonas sp. Nea-C	-0.55±0.04	n.a	n.a	Ehrl et al. (2018)
Polaromonas sp. Nea-C (cell-free extract)	-0.60±0.14	n.a	n.a	Ehrl et al. (2018)
Sinorihizobium sp. K	-1.07±0.14	n.a	n.a	Chen et al. (2017)
Chelatobacter heintzii	-0.65±0.08	n.a	n.a	Meyer et al. (2008)
Ensifer sp.	-0.55±0.05	n.a	n.a	Ehrl et al. (2018)
Rhizobium sp. CX-Z	-0.37±0.02	n.a	n.a	Chen et al. (2019a)
Wild type TrzN	-0.55±0.02	n.a	n.a	Schürner et al. (2015)
Biotic hydrolysis	-0.55±0.02	1.7±0.9	-1.2±0.7	*combined data*
Rhodococcus sp. NI86/21	0.66±0.12	0.62±0.14	0.36±0.16	Lihl et al. (2020)
Rhodococcus sp. NI86/21	0.36±0.06	n.a	n.a	Meyer et al. (2014)

Oxidative dealkylation	0.66±0.04	0.62±0.14	0.36±0.16	*combined data*
Oxidation by indirect photolysis by 4-carboxybenzophenone or OH· radical	0.43±0.04	n.a	n.a	Hartenbach et al. (2008)
Direct photolysis	1.03±0.11	n.a	n.a	Hartenbach et al. (2008)
Oxidation with permanganate	0.01±0.005	n.a	n.a	Meyer et al. (2014)

[a]estimated as ~$\varepsilon_C/\varepsilon_{Cl}$; using values from Meyer et al. (2009) and Grzybkowska et al. (2014), respectively.

Table S15. Z-scores and corresponding p-values using two-tailed hypothesis testing for all possible pairings of dual isotope slopes ($\Lambda_{N/C}$, $\Lambda_{C/Cl}$ and $\Lambda_{N/Cl}$) for ATR. All comparisons were considered statistically significant at the $\alpha < 0.05$ level. Our data and data from previous studies are used, as detailed in **Table S14**. Acidic and alkaline refers to hydrolysis at pH 3 and pH 12, respectively, at 25°C. Biotic refers to biotic hydrolysis by different bacteria strains. Dealkylation refers to oxidative dealkylation by *Rhodococcus* sp. NI86/21. Indirect photolysis refers to oxidation by indirect photolysis by 4-carboxybenzophenone or OH· radical. Photolysis refers to direct photolysis. Permanganate refers to oxidation by permanganate.

Compared slopes	z-score	p-value	Significant different ($\alpha = 0.05$)
$\Delta\delta^{15}N/\Delta\delta^{13}C$ plot			
Acidic vs Alkaline	-20.963	<0.00001	Yes
Biotic vs Alkaline	-31.921	<0.00001	Yes
Dealkylation vs Alkaline	6.352	<0.00001	Yes
Biotic vs Acidic	**-0.972**	**0.33254**	**No**
Dealkylation vs Acidic	16.775	<0.00001	Yes
Biotic vs Dealkylation	-18.828	<0.00001	Yes
Dealkylation vs Indirect photolysis	**1.646**	**0.10764**	**No**
Alkaline vs Indirect photolysis	-5.205	<0.00001	Yes
Biotic vs Indirect photolysis	-20.074	<0.00001	Yes
Acidic vs Indirect photolysis	-17.279	<0.00001	Yes
Dealkylation vs Photolysis	-4.126	0.00026	Yes
Alkaline vs Photolysis	-7.912	<0.00001	Yes
Biotic vs Photolysis	-14.691	<0.00001	Yes
Acidic vs Photolysis	-13.994	<0.00001	Yes
Indirect photolysis vs Photolysis	-5.283	0.00009	Yes
Dealkylation vs Permanganate	9.713	<0.00001	Yes
Alkaline vs Permanganate	15.684	<0.00001	Yes
Biotic vs Permanganate	-26.434	<0.00001	Yes
Acidic vs Permanganate	-16.299	<0.00001	Yes
Indirect photolysis vs Permanganate	9.333	<0.00001	Yes
Photolysis vs Permanganate	9.623	<0.00001	Yes
$\Delta\delta^{13}C/\ \Delta\delta^{37}Cl$ plot			
Acidic vs Alkaline	**1.762**	**0.07808**	**No**
Biotic vs Alkaline	**-1.762**	**0.07811**	**No**
Dealkylation vs Alkaline	-2.429	0.01515	Yes
Biotic vs Acidic	-9.287	<0.00001	Yes
Dealkylation vs Acidic	13.357	<0.00001	Yes
Biotic vs Dealkylation	2.655	0.00792	Yes
$\Delta\delta^{15}N/\Delta\delta^{37}Cl$ plot			
Acidic vs Alkaline	-7.595	<0.00001	Yes
Biotic vs Alkaline	-4.233	0.00002	Yes
Dealkylation vs Alkaline	-2.166	0.03034	Yes
Biotic vs Acidic	5.284	<0.00001	Yes
Dealkylation vs Acidic	-8.395	<0.00001	Yes
Biotic vs Dealkylation	-4.803	<0.00001	Yes

Table S16. Eigenvectors and standard error for the first principal component of the covariance matrix for each isotope fractionation trend. Principal component analysis in SigmaPlot v.14.0 was used following Palau et al. (2017). Data for biotic hydrolysis by *Arthrobacter aurescens* TC1 and for oxidative dealkylation by *Rhodococcus* sp. NI86/21 are from Lihl et al. (2020). Characteristic unit vectors for each degradation pathway are shown in **Figure 4** in the main text.

	$\Delta\delta^{37}Cl$	$\Delta\delta^{13}C$	$\Delta\delta^{15}N$
Acidic hydrolysis	0.103 ± 0.009	0.849 ± 0.009	-0.518 ± 0.016
Alkaline hydrolysis	0.138 ± 0.037	0.943 ± 0.013	0.302 ± 0.035
Biotic hydrolysis	0.282 ± 0.059	0.787 ± 0.021	-0.549 ± 0.029
Oxidative dealkylation	0.797 ± 0.032	0.517 ± 0.028	0.314 ± 0.043

To further assess the similarities and differences between the unit vectors, the angle θ between two of these vectors can be calculated following the method described in Palau et al. (2017) by applying this equation:

$$\cos\theta = \frac{\vec{V}\cdot\vec{U}}{|\vec{V}|.|\vec{U}|} = \frac{v_1u_1+v_2u_2+v_3u_3}{\sqrt{v_1^2+v_2^2+v_3^2}.\sqrt{u_1^2+u_2^2+u_3^2}} \quad \textbf{Eq (S4)}$$

With (v_1, v_2, v_3) and (u_1, u_2, u_3) the coefficients of unit vectors $\underset{V}{\rightarrow}$ and $\underset{U}{\rightarrow}$, respectively. These angles can be used to assess the difference between two degradation pathways associated to two vectors. The larger the angle, the more different the two vectors are. The values for these angles are summarized in **Table S17**. The uncertainty of the angles θ was estimated by error propagation. All the angles are > 10°, indicating that all unit vectors are different, and therefore that all considered degradation pathways can be distinguished from each other.

Table S17. Values of the angle between all possible pairing of eigenvectors shown in **Figure 4** in the main text.

Compared vectors	Cos θ	Angle θ (°)	Error (°)
Acidic vs alkaline hydrolysis	0.659	49	1
Acidic vs biotic hydrolysis	0.982	11	7
Acidic vs dealkylation	0.358	69	1
Alkaline vs biotic hydrolysis	0.615	52	1
Alkaline hydrolysis vs dealkylation	0.692	46	2
Biotic hydrolysis vs dealkylation	0.459	63	1

10. References

Aeppli, C., H. Holmstrand, P. Andersson, and Ö. Gustafsson. 2010. Direct Compound-Specific Stable Chlorine Isotope Analysis of Organic Compounds with Quadrupole GC/MS Using Standard Isotope Bracketing. *Analytical Chemistry* 82 no. 1: 420-426.

Alvarez-Zaldívar, P., Payraudeau, S., Meite, F., Masbou, J., Imfeld, G. 2018. Pesticide degradation and export losses at the catchment scale: Insights from compound-specific isotope analysis (CSIA). *Water Research*, 139, 198-207.

Arcelli, A., M. Papa, G. Porzi, and S. Sandri. 1997. Participation of neighbouring amide group in the competitive acid catalysed hydrolysis of ether linkage and an intramolecular SN2 reactions. 2. *Tetrahedron* 53 no. 30: 10513-10516.

Carlson, D.L., K.D. Than, and A.L. Roberts. 2006. Acid- and Base-Catalyzed Hydrolysis of Chloroacetamide Herbicides. *Journal of Agricultural and Food Chemistry* 54 no. 13: 4740-4750.

Chen, S., K. Zhang, R.K. Jha, and L. Ma. 2019. Impact of atrazine concentration on bioavailability and apparent isotope fractionation in Gram-negative Rhizobium sp. CX-Z. *Environmental Pollution* 257: 113614.

Droz, B., Drouin, G., Maurer, L., Villette, C., Payraudeau, S., and Imfeld, G. 2021. Phase-Transfer and Biodegradation of Pesticides in Water–Sediment Systems Explored by Compound-Specific Isotopes Analysis and Conceptual Modeling. *Environmental Science & Technology* 55: 4720-4728.

Ehrl, B.N., M. Gharasoo, and M. Elsner. 2018. Isotope Fractionation Pinpoints Membrane Permeability as a Barrier to Atrazine Biodegradation in Gram-negative Polaromonas sp. Nea-C. *Environmental Science & Technology* 52 no. 7: 4137-4144.

Ehrl, B.N., K. Kundu, M. Gharasoo, S. Marozava, and M. Elsner. 2019. Rate-Limiting Mass Transfer in Micropollutant Degradation Revealed by Isotope Fractionation in Chemostat. *Environmental Science & Technology* 53 no. 3: 1197-1205.

Grzybkowska, A., R. Kaminski, and A. Dybala-Defratyka. 2014. Theoretical predictions of isotope effects versus their experimental values for an example of uncatalyzed hydrolysis of atrazine. *Physical Chemistry Chemical Physics* 16 no. 29: 15164.

Hartenbach, A.E., T.B. Hofstetter, P.R. Tentscher, S. Canonica, M. Berg, and R.P. Schwarzenbach. 2008. Carbon, Hydrogen, and Nitrogen Isotope Fractionation During Light-Induced Transformations of Atrazine. *Environmental Science & Technology* 42 no. 21: 7751-7756.

Hunkeler, D., P. Höhener, S. Bernasconi, and J. Zeyer. 1999. Engineered in situ bioremediation of a petroleum hydrocarbon-contaminated aquifer: assessment of mineralization based on alkalinity, inorganic carbon and stable carbon isotope balances. *Journal of Contaminant Hydrology* 37 no. 3: 201-223.

Kochany, J. and R. J. Maguire. 1994. Sunlight Photodegradation of Metolachlor in Water. *Journal of Agricultural and Food Chemistry* 42 no.2: 406-412.

LeBaron, H.M., McFarland, J.E., Simoneaux, J.B. and Ebert E. 1988. Metolachlor. In *Herbicides: Chemistry, Degradation and Mode of Action*, ed. P.C. Kearney and D.D. Kaufman, Vol. 3, pp. 335-382. Marcel Dekker, New York.

Lerch, R. N. and W. W. Donald. 1994. Analysis of Hydroxylated Atrazine Degradation Products in Water Using Solid-Phase Extraction and High-Performance Liquid Chromatography. Journal of Agricultural and Food Chemistry 42 no 9: 2074-2074.

Lihl, C., B. Heckel, A. Grzybkowska, A. Dybala-Defratyka, V. Ponsin, C. Torrentó, D. Hunkeler, and M. Elsner. 2020. Compound-Specific Chlorine Isotope Fractionation in Biodegradation of Atrazine. *Environmental Science: Processes & Impacts* 22: 792-801.

Lihl, C., J. Renpenning, S. Kümmel, F. Gelman, H. Schuerner, M. Daubmeier, B. Heckel, A. Melsbach, A. Bernstein, O. Shouakar-Stash, M. Gehre, and M. Elsner. 2019. Towards improved accuracy in chlorine isotope analysis: synthesis routes for in-house standards and characterization via complementary mass spectrometry methods. *Analytical Chemistry* 91 no. 19: 12290-12297.

Masbou, J., G. Drouin, S. Payraudeau, and G. Imfeld. 2018. Carbon and nitrogen stable isotope fractionation during abiotic hydrolysis of pesticides. *Chemosphere* 213: 368-376.

Meite, F. 2018. Transformation and transport of inorganic and synthetic pesticides in soils of agricultural catchments. PhD Thesis, Université de Strasbourg, 2018, 407 p.

Meyer, A.H., A. Dybala-Defratyka, P.J. Alaimo, I. Geronimo, A.D. Sanchez, C.J. Cramer, and M. Elsner. 2014. Cytochrome P450-catalyzed dealkylation of atrazine byRhodococcussp. strain NI86/21 involves hydrogen atom transfer rather than single electron transfer. *Dalton Transactions* 43 no. 32: 12175-12186.

Meyer, A.H., H. Penning, and M. Elsner. 2009. C and N Isotope Fractionation Suggests Similar Mechanisms of Microbial Atrazine Transformation Despite Involvement of Different Enzymes (AtzA and TrzN). *Environmental Science & Technology* 43 no. 21: 8079-8085.

Meyer, A.H., H. Penning, H. Lowag, and M. Elsner. 2008. Precise and Accurate Compound Specific Carbon and Nitrogen Isotope Analysis of Atrazine: Critical Role of Combustion Oven Conditions. *Environmental Science & Technology* 42 no. 21: 7757-7763.

Ojeda, A.S., Phillips, E., Mancini, S.A., Lollar, B.S. 2019. Sources of Uncertainty in Biotransformation Mechanistic Interpretations and Remediation Studies using CSIA. *Analytical Chemistry* 91 no. 14: 9147-9153.

Palau, J., O. Shouakar-Stash, S. Hatijah Mortan, R. Yu, M. Rosell, E. Marco-Urrea, D.L. Freedman, R. Aravena, A. Soler, and D. Hunkeler. 2017. Hydrogen Isotope Fractionation during the Biodegradation of 1,2-Dichloroethane: Potential for Pathway Identification Using a Multi-element (C, Cl, and H) Isotope Approach. Environmental Science & Technology 51 no. 18: 10526-10535.

Pérez-Rodríguez, P., Schmitt, A.D., Gangloff, S., Masbou, J., Imfeld, G. 2021) Plants affect the dissipation and leaching of anilide pesticides in soil mesocosms: Insights from compound-specific isotope analysis (CSIA). *Agriculture, Ecosystems & Environment* 308: 107257.

Plust, S.J., J.R. Loehe, F.J. Feher, J.H. Benedict, and H.F. Herbrandson. 1981. Kinetics and mechanism of hydrolysis of chloro-1,3,5-triazines. Atrazine. *The Journal of Organic Chemistry* 46 no. 18: 3661-3665.

Ponsin, V., C. Torrento, C. Lihl, M. Elsner, and D. Hunkeler. 2019. Compound-specific chlorine isotope analysis of the herbicides atrazine, acetochlor and metolachlor. *Analytical Chemistry* 91 no. 22: 14290-14298.

Prosen, H., and L. Zupančič-Kralj. 2005. Evaluation of photolysis and hydrolysis of atrazine and its first degradation products in the presence of humic acids. *Environmental Pollution* 133 no. 3: 517-529.

Ripley, B.D., Clegg, B.S., Porter, C.S., and Chapman, N.D. 1986. Hydrolysis of Acylalanine Fungicides and Chloroacetamide Herbicides. *Abstracts: Sixth International Congress of Pesticide Chemistry*, IUPAC, 10–15 Aug., 1986: 6B–17.

Schürner, H.K.V., J.L. Seffernick, A. Grzybkowska, A. Dybala-Defratyka, L.P. Wackett, and M. Elsner. 2015. Characteristic Isotope Fractionation Patterns in s-Triazine Degradation Have Their Origin in Multiple Protonation Options in the s-Triazine Hydrolase TrzN. *Environmental Science & Technology* 49 no. 6: 3490-3498.

Torrentó, C., R. Bakkour, G. Glauser, A. Melsbach, V. Ponsin, T.B. Hofstetter, M. Elsner, and D. Hunkeler. 2019. Solid-phase extraction method for stable isotope analysis of pesticides from large volume environmental water samples. *Analyst* 144 no. 9: 2898-2908.